https://doi.org/10.5194/egusphere-2025-1770
Preprint. Discussion started: 11 June 2025

Detection of dietary stress and geophagic behaviour forced by dry seasons in Miocene *Gomphotherium*

Rute Coimbra [(a)], Niels de Winter [(b,c)], Maria Ríos [(d, e)], Rui Bernardino[(f)] , Darío Estraviz-López [(d, e)], Priscila Lohmann [(d)], Roberta Martino [(d, e)], Aurora Grandal-d'Anglade [(g)], Fernando Rocha [(a)], Philippe Claeys [(c)]

(a) Geobiotec, Dpt. of Geosciences, University of Aveiro, Portugal

(b) Dept. of Earth Sciences, Vrije Universiteit Amsterdam, Netherlands

(c) Archaeology, Environmental Changes & Geo-chemistry group, Vrije Universiteit Brussel, Belgium

(d) Dpt. of Earth Sciences, NOVA School of Science and Technology, Universidade Nova de Lisboa, GeoBioTec, Caparica, Portugal

(e) Museu da Lourinhã, Lourinhã, Portugal

(f) Jardim Zoológico de Lisboa, Lisboa, Portugal

(g) ESCI, Instituto Universitario de Xeoloxía, Universidade da Coruña, A Coruña, Spain

Corresponding author and first author:

Rute Coimbra rcoimbra@ua.pt

Abstract

To access the impact of anthropogenic emissions and land use change on Earth's climate and biodiversity, studies into the environment and ecology of natural ecosystems during past warm periods are required. The Miocene Climatic Optimum is a key reference period for future global warming scenarios. However, studies uncovering Miocene climate have heavily favoured marine environments, leaving the impact of warming on terrestrial ecosystems understudied. Here, we present a multi-disciplinary study into the chemical composition of fossil *Gomphotherium angustidens* (Proboscidea, Mammalia) teeth from the Middle Miocene Vb division (~15.9–16.1Ma) of western Portugal (Chelas Valley, Lisbon, Lusitanian basin) and their sedimentological context. Trace element and stable isotope compositions in these fossil teeth are compared with similar measurements in molars of a taxonomically related modern African elephant (captive *Loxodonta africana*). Results reveal seasonal-scale variability in trace elements in both fossil and modern proboscidean tooth enamel, which are interpreted as evidence for seasonal changes in diet. Periodic increases in Na, Fe and Si in *G. angustidens* demonstrate intake of sediment in the diet during fixed times of the year, a behaviour type previously described in modern elephants during dry seasons. In combination with the heavier carbon and oxygen isotopic composition in *G. angustidens* compared to *L. africana*, the terrestrial climate in Miocene Portugal appears characterized by seasonally dry periods, which forced geophagy behaviour of these large mammals and likely had significant consequences for the composition of Miocene ecosystems (e.g., food/water availability and potential seasonal range shifts) in southwestern Europe.

https://doi.org/10.5194/egusphere-2025-1770
Preprint. Discussion started: 11 June 2025

1. Introduction

1.1 The Middle Miocene as a reference period for warm climate

The study of historical variations in climate and environment has emerged as a potent method for understanding the scale, duration, and trajectory of global change. This approach also aids in assessing and forecasting potential outcomes in future scenarios, as underscored by the Intergovernmental Panel on Climate Change (IPCC) in its 6th assessment report (IPCC, 2023). The Middle Miocene Climate Optimum (MCO; 17 – 15 Ma) represents a period of major global warming within the Cenozoic cooling trend (Domingo et al., 2009; Harzhauser et al., 2011; Meckler et al., 2022; Westerhold et al., 2020). This brief hot period, reaching ~ 600 ppm atmospheric CO_2, closely mimics projections for future temperatures under a moderate IPCC warming (Meinshausen et al., 2020; Methner et al., 2020; Super et al., 2018). Therefore, MCO constitutes an appropriate analogue to access the predictive nature of climate models (Burls et al., 2021; Goldner et al., 2014; Holbourn et al., 2015; Steinthorsdottir et al., 2020).

Employing biogeochemical techniques to extract short-term geochemical information from fossil skeletal remains constitutes a highly informative method, as it enables the characterization of past global changes for a timespan that far exceeds instrumental records (Meckler et al., 2022; Westerhold et al., 2020; Zachos et al., 2001, 2008). A deeper exploration of the marine geological record has been carried out from a biogeochemical perspective, specifically utilizing stable oxygen isotope ratios ($\delta^{18}O$) as proxies for past ocean water density (salinity and/or temperature). The $\delta^{18}O$ proxy has been primarily used in the study of marine paleoarchives (Westerhold et al., 2020; Zachos et al., 2008). Since a similarly detailed approach is missing from the continental realm, it is crucial to enhance biogeochemical investigations into proxies reflecting terrestrial records to achieve a comprehensive understanding of the climatic, environmental, and ecological changes that have shaped the planet.

1.2 Bioapatite as an environmental archive

Bioapatite ($Ca_{10}(PO_4, CO_3)_6(OH, F)$; LeGeros, 1986), the material from which teeth and bones in terrestrial vertebrates are made, constitutes a promising archive for recording short-term environmental variability in the terrestrial realm. Bioapatite is one of the strongest biogenic materials and has excellent fossilization potential (Lee-Thorp and Sponheimer, 2003). The oxygen isotope composition of carbonate ($\delta^{18}O_c$) structurally bound to bioapatite in skeletal tissues primarily reflects the climatic and environmental conditions experienced by the examined individual during its life (Cerling et al., 1997a; de Winter and Claeys, 2016; Fricke and O'Neil, 1996). For terrestrial vertebrates, these measurements mirror the $\delta^{18}O$ content of body water, which, in turn, captures the $\delta^{18}O$ composition of meteoric water after correcting for metabolic fractionation, and are related to the mineralization temperature of the mineral (Ayliffe et al., 1992). Furthermore, with increasing aridity, the enrichment of ^{18}O in meteoric and vegetation water, and therefore in tooth enamel, intensifies due to evaporation effects- Rayleigh fractionation (Tütken et al., 2007). Hence, the bioapatite $\delta^{18}O_c$ signature found in fossil vertebrates serves as a valuable source of information about temperature and aridity levels within terrestrial environments (Koch et al., 2007).

Initial investigations into the carbon isotope value of bioapatite ($\delta^{13}C_{ap}$) in terrestrial vertebrates revealed its capacity to document dietary choices, facilitating the reconstruction of habitats (such as forested versus open areas). In the context of herbivore species, $\delta^{13}C_{ap}$ values are influenced by the photosynthetic pathway of consumed plants, enabling differentiation among C3, C4, and Crassulacean Acid Metabolism (CAM) metabolic pathways (Koch et al., 2007).

The recent development of high-resolution micro-XRF (µXRF) line scanning to analyze trace element abundances on cleaned surfaces of mammal molars serves as a valuable complement to conventional isotope proxies (de Winter et al., 2019; de Winter and Claeys, 2016). The findings demonstrate a link between seasonal fluctuations and trace element patterns in enamel, namely in Sr/Ca, Zn/Ca, K/Ca, Fe/Ca and S/Ca. These ratios reflect the intake of trace elements through dust (discerning between summer and winter) or dietary modifications. The documented connection constitutes a promising avenue for utilizing these trace element ratios as a novel proxy to explore seasonal fluctuations in both the ancient environment and dietary habits of extinct Proboscideans, potentially applicable to other mammalian species (de Winter et al., 2017; Kohn and Cerling, 2002) .

1.3 Proboscidean teeth as archives for terrestrial environmental variability and paleobiology

Mammal tooth enamel has emerged as a valuable recorder of paleo-seasonality due to its resistance to diagenesis and its sequential growth, facilitating the retrieval of records with exceptional temporal resolution (Blaise and Balasse, 2011). An additional benefit of employing mammal teeth for sub-annual environmental reconstructions is the potential to amalgamate several teeth from a single individual, forming a composite time series. This combination enables the generation of extended, uninterrupted records depicting fluctuations in paleoenvironmental conditions throughout the years when the teeth underwent mineralization (De Winter et al., 2016; Kohn and Cerling, 2002).

Proboscideans, which are among the largest land herbivores of the Neogene era (Fig. 1A), are polyphyodonts, undergoing cycles of tooth replacement over their lifetimes (Lee et al., 2012). New teeth gradually develop at the rear of the mouth, moving forward to displace and replace the anteriorly located older ones (molar progression; Fig. 1B) (Lee et al., 2012; Metcalfe and Longstaffe, 2012). Their molars are lophodont (Fig. 1C and D), composed of enamel lophs filled with dentin and surrounded by cementum (Lee et al., 2012). Throughout the process of tooth formation, the growth of enamel initiates at the front of the crown and advances in a loph-by-loph manner towards the distal end of the tooth and the root. This progression continues until it reaches the point where the crown and root meet, offering a distinct pathway for conducting analyses of seasonality (Fig. 1). The rates at which enamel accumulates in proboscidean molars suggest the possibility of capturing an environmental record spanning up to 15 years (Metcalfe and Longstaffe, 2012), with an enamel accretion rate up to ~13 mm/yr (Dirks et al., 2012; Esker et al., 2019; Kowalik et al., 2023). Proboscideans possess a diverse evolutionary lineage and extensive fossil record, rendering them a captivating subject of study. This characteristic offers the potential for terrestrial paleoclimate reconstruction, spanning from the Late Paleocene era to the present day (Cantalapiedra et al., 2021; Liu et al., 2008).

1.4 *G. angustidens* and modern elephant evolution and biogeography

Gomphotherium (Fig. 1A) is an extinct genus of gomphothere proboscidean, which once roamed the Neogene landscapes of Eurasia, Africa, and North America (Wang et al., 2014). Its origin can be traced back to Africa during the late Oligocene to early Miocene period (Wang et al., 2017). The earliest remnants of *Gomphotherium*, date back approximately 19.5 million years, and were discovered in Africa (Wang et al., 2017). Around 19 million years ago, *Gomphotherium* embarked on a range shift into Eurasia via the "*Gomphotherium* Land Bridge”, a land bridge that connected Eurasia to Afro-Arabia (Harzhauser et al., 2007). Upon its arrival in Eurasia, *Gomphotherium* experienced rapid evolutionary changes, reaching its zenith of diversity during the Early-Middle Miocene epoch. As the Pliocene dawned, the last known *Gomphotherium* species vanished from North America, around 5 million years ago (MacFadden et al., 2015).

Most *Gomphotherium* species reached a size comparable to the modern Asian elephant. They were characterized by their distinctive long lower jaw tusks and four-tusked dentition (Larramendi, 2015). Gomphotheres inhabited a diverse range of habitats, and while the majority of *Gomphotherium* species are believed to have been browsers, indications suggest that certain specimens of *G. steinheimense* from China showed grazing habits (Wu et al., 2018). Modern elephants are primarily considered browsers, rather than grazers, although they do consume grasses as part of their diet, especially during times of food scarcity (Wu et al., 2018).

https://doi.org/10.5194/egusphere-2025-1770
Preprint. Discussion started: 11 June 2025

The evolution of elephantids is believed to have stemmed from gomphotheres, and the forebears of modern elephants might be African members of the "tetralophodont gomphothere" *Tetralophodon* (Geraads et al., 2019). The family's earliest members date back to the Late Miocene period, approximately 9-10 million years ago (Saegusa et al., 2014). While early members of Elephantidae had lower tusks, these were lost in later members as the feeding function of the mandible shifted gradually to the trunk, possibly as an adaptation to slightly more grazing habits (Li et al., 2023; Mothé et al., 2016). By the end of the Miocene epoch, elephants and mammoths diverged from each other, and during the Pliocene the elephantid range shift from Africa started, leading to the arrival of mammoths and *Elephas* in Eurasia approximately 3.8-3 million years ago (Iannucci and Sardella, 2023).

One critical aspect of proboscidean evolution was the modification of their check teeth occlusal morphology, which changed from the low-crowned bunolophodont molars of the trilophodont *Gomphotherium* with few lophs, to the high-crowned and multi-plated teeth of the more derived elephantiforms such as *Loxodonta* (Wu et al., 2018). This evolution is of relevance because such dental change allowed them to consume more abrasive foods with the establishment of C4 vegetation between 8 to 5 Ma (Wu et al., 2018). While these changes in the morphological and ecological context may cause some differences in the composition of teeth from extant and the extinct specimens, comparison between modern elephants and the Middle Miocene *Gomphotherium* still contributes to our understanding of how modern elephants and their ancestors adapted and diversified over the last millions of years.

1.5 *Gomphotherium* dietary and environmental changes in Middle Miocene climate

This study presents a comparison between seasonal patterns in trace element concentrations of and extant elephants and extinct Middle Miocene *Gomphotherium*. The Miocene record in Portugal provides favourable conditions for conducting this research on fossil *Gomphotherium* specimens (Antunes and Pais, 1984; Pais et al., 2012), since it is supported by a robust stratigraphic framework and detailed depositional sequences, biostratigraphy and isotopic dating based on marine fossils, while also exhibiting a substantial connection with terrestrial sedimentary formations.

The Middle Miocene *G. angustidens* material described here was collected in Portugal (Lisbon region; Fig. 2A B and C). The specimens lived prior to the establishment of C4 vegetation, which happened around 8-5 million years ago (Cerling et al., 1997a), and before the emergence of Elephantidae from the ancestral stock of Miocene gomphotheres (Cerling and Harris, 1999). This temporal division coincides with the Middle Miocene Climatic Optimum (MMCO), which occurred approximately 14 to 17 million years ago. During this period, the Earth experienced relatively warmer and more stable climatic conditions, with higher temperatures than immediately before or after this interval. The MMCO was characterized by reduced polar ice and relatively uniform temperatures across latitudes, making it a period of significant climatic stability during the Miocene epoch (Westerhold et al., 2020; Zachos et al., 2001).

Climatic assessments based on marine samples from the Middle Miocene of the Lower Tagus Basin (LTB) indicate prevailing tropical conditions in the studied region (Pais et al., 2012). During the Upper Burdigalian and Langhian stages(~17 – 15 Ma), water temperatures reached a peak, resembling the present-day climate of the Guinea Gulf (Pais et al., 2012). On land, Portuguese records indicate a decline in both humidity and temperature, leading to the prevalence of savanna or steppe habitats with gallery forests found alongside rivers (Pais et al., 2012). Subsequently, temperatures declined. Evidence from continental faunas and sediments indicates a cyclical alternation of moist and arid periods, , with the Langhian stage (~16.5 – 15 Ma) being the driest (Antunes and Pais, 1984; Pais et al., 2012).

https://doi.org/10.5194/egusphere-2025-1770
Preprint. Discussion started: 11 June 2025

2. Materials

2.1 *Gomphotherium angustidens*

Insights into continental Miocene landscapes are derived from the analysis of molars, representing the extinct proboscidean. The selected *G. angustidens* specimens were collected at Quinta da Farinheira, Chelas Valley (Fig. 2B), falling within the Cotter (1956) subdivision Vb, and the subdivision SDL1 ((~15.9–16.1 million years ago (Antunes and Ginsburg, 2003). It belongs to the Middle Miocene Langhian stage and the MN5 biozone and the final part of MN4 (13.7–16.0 Ma; Fig. 2C). The encasing friable reddish terrigenous material presents reddish hues (Fig. 2D and E) provides ideal conditions to extract the molars of interest without risking mechanical damage. This subdivision includes the Burdigalian and Langhian stages (Pais et al., 2012). The specimens are curated at the Department of Earth Sciences of the Universidade NOVA de Lisboa and are molars accessioned with the numbers: FCT-DCT-4943, FCT-DCT-4944, and FCT-DCT-4945 (Fig. 3A to C and Fig. 4).

2.2 *Loxodonta africana*

The extant proboscidean analogue material belongs to the African elephant *Loxodonta africana*. It was provided by Jardim Zoológico de Lisboa (Lisbon Zoo) and consists of a complete molar tooth (Fig. 3D and Fig. 4) also deposited at the Department of Earth Sciences of the Universidade NOVA de Lisboa (FCT-DCT-4946). It belongs to an adult individual, born in the wild and later moved into an enclosed environment in the Lisbon Zoo until its death, at the end of the 20th century. It is not uncommon to find fallen elephant molars amongst hay and other materials during cleaning activities at the Zoo. This is the case of the sample used in this study, accounting for the uncertainty regarding to which individual they belonged to, as well as if the molar was mineralized in the wild or during captivity. Since a few decades, the Lisbon Zoo shelters African elephants born and raised in the wild as well as others born under their care, a clear reflection of their reproductive success under optimum conditions. Animal enrichment includes (among many others) a tight control on substrate (soil) composition, requiring periodic addition of external components from variable sources to stimulate natural behaviours.

3. Methods

3.1 Sample preparation

Three molars, likely of different individuals, of *G. angustidens* (FCT-DCT 4943, FCT- DCT 4944 and FCT-DCT 4945) and one molar of *L. africanus* (FCT-DCT 4946)(examples in Fig. 3 and 4) were cut in mesio-distal (anterior-posterior) direction, perpendicular to the orientation of the lophs in *L. africana* and the cusp rows in *G. angustidens*, to reveal a cross section through the cusps of the molars (following Uno et al., 2020). Cross sections were polished using CeO_2 powder suspension to ensure a flat surface for µXRF scanning (Fig. 4). Sectioning through the molars, while destructive, targeted the enamel in the cusps/lophs using µXRF line scanning to obtain time series of trace element composition through the teeth (see **section 3.4**).

3.2 Mineralogical analysis of soil samples

To characterize the chemical components of soil potentially contributing to the composition of the molar enamel during mineralization and/or diagenetic evolution, the mineralogical composition of soil samples associated with both modern and fossil molars used in this study was analysed. Samples were taken from sediment material found directly around the molars and inside the cavities between the cusps. In samples associated with modern elephant models, soil particles were isolated from the organic matter in material lodged between the molar cusps by soaking samples in deionized water and decanting the liquid and floating constituents from the samples. In this way, only soil particles were taken into account for further analysis. Sediment samples associated with fossil and modern molars were analysed using X-Ray Diffraction (XRD) with Cu-Kα radiation, carried out using PANALYTICAL Phillips X'Pert PW3040/60 equipment, with the X´Pert 2.0 and Profit software (Department of Geosciences, University of Aveiro, Portugal). Scans were run between 4 and 65° 2θ for bulk samples and between 2 and 40° 2θ of non-oriented powder mounts of fine fractions for clay mineral identification. Divergence slit was fixed at 1.0, receiving slit at 0.20; the scan step size of 0.02 for 3050 points at continuous scan; time per step was 1 sec/2θ. Fine fraction analysis was carried out in the air-dry state and after glycerol saturation and heat treatment (500°C). Peak identification and semi-quantitative estimation were performed using HighScore software (Malvern Panalytical v. 4.9; ICDD database-International Centre for Diffraction Data). Identification of the different mineral phases followed the criteria recommended by (Brown and Brindley, 1980; Schultz, 1964) and the Joint Committee for Powder Diffraction Standards. Semi-quantitative mineralogical analyses followed the criteria recommended by (Mellinger, 1979; Schultz, 1964; Thorez, 1976); peak areas of the specific reflections were calculated and weighted by empirically estimated factors, according to (Galhano et al., 1999; Oliveira et al., 2002).

3.3 Trace element maps and profiles

3.3.1 Instrument setup

Concentrations of Ca, P, Na, Mg, Sr, S, Si, Fe, Al, K and Mn are determined across sections through proboscidean molars using an energy-dispersive Bruker M4 Tornado µXRF scanner (Bruker nano GmbH, Berlin, Germany) at AMGC in Brussels. The XRF spectra produced enable detection and quantification of a wide array of elements (see de Winter and Claeys, 2016), however, the discussion is limited to the selected elements referred above. This selection was based on the degree of significance during elemental data processing (details in Appendix). We first mapped the entire cross section of each specimen using semi-quantitative mapping to identify the best-preserved areas in the fossil teeth by comparison between fossil and modern specimens. Then, we targeted those well-preserved enamel sections using quantitative elemental profiling (examples in Fig. 5).

The Bruker M4 Tornado features a Rh-anode X-ray source operated at 50 mV and 600 µA (30 W) and two 30 mm^2 silicon drift detectors mounted in a low vacuum (20 mbar) chamber under a precise orientation such that the incoming and outgoing (detected) X-ray radiation describe a 90° angle when they hit the sample (see de Winter and Claeys, 2016). The X-rays from the source are focused using a poly-capillary lens. This configuration ensures that exciting X-rays can be focused on a round ~25 µm diameter spot on the polished sample surface (calibrated for Mo-kα radiation), which is mounted on a XYZ moving stage to allow collection of a spatial array of XRF spectra. Peaks in XRF spectra belonging to elements of interest are identified and integrated using Bruker Esprit software, which includes a deconvolution algorithm for estimating the relative contributions of overlapping peaks in the XRF spectrum.

3.3.2 µXRF mapping

The entire surface of all cross sections is mapped using µXRF to produce semi-quantitative maps of trace element distribution. For µXRF maps, the X-ray source is moved along the sample surface continuously in a raster pattern while XRF spectra accumulate in 25 µm by 25 µm pixels with a total integration time of 1 ms (following de Winter and Claeys, 2016). This sampling strategy does not allow enough integration time for spectrum-by-spectrum quantification of trace element concentrations, but instead produces semi-quantitative element distribution maps by creating false-colour images of the deconvoluted surface area under element peaks (Fig. 5 and https://doi.org/10.5281/zenodo.14882824). These maps were not used to determine accurate concentrations of elements in the specimens, but used to guide the optimal location for quantitative XRF line scanning.

3.3.3 µXRF line scanning

Quantitative µXRF trace element profiles are measured along the exposed enamel in cross sections through the cusps and lophs of the proboscidean molars (see Fig. 3). We apply point-by-point line scanning (following (Vansteenberge et al., 2020), allowing the detectors to count fluorescent X-rays returning from the sample for 60 seconds per point (following de Winter and Claeys, 2016). This approach allows enough measurement time per point to reach the Time of Stable Accuracy and Time of Stable Reproducibility recommended in (de Winter et al., 2017), thereby achieving a compromise between spectrum quality, measurement time and spatial resolution of the trace element profiles. Trace element concentrations are quantified using the matrix-matched bioapatite calibration developed in (De Winter et al., 2016) using a combination of in-house and certified bioapatite standards. This method achieves measurement errors better than 10% for all elements considered in this study (see detailed error analysis in de Winter and Claeys, 2016).

3.4 Stable isotope analyses

After carrying out the µXRF analyses, enamel samples were drilled using a hand-held dental drill (Dremel equipped with a 3 mm drill-bit) from the cross sections through the molars for stable carbon ($\delta^{13}C$) and oxygen ($\delta^{18}O$) isotope analyses of the structurally bound carbonate in the tooth bioapatite, performed at Universidade da Coruña (A Coruña, Spain). Bioapatite samples (N = 42) were drilled from multiple parallel cusps and various heights along the cusps within the molars to quantify inter-tooth variability in isotopic composition. Approximately 1 mg of enamel powder was used for stable isotope analyses. No pre-treatment is carried out since the samples were obtained from clean cross sections through the molars and were considered unlikely to have been in contact with diagenetic fluids considering the taphonomic history of the sample site (see **section 2**). Therefore, the risk of introducing diagenetic (labile) carbonate fractions in the samples was sufficiently low to motivate the choice not to use pre-treatment techniques, which have been demonstrated to affect the original isotopic composition of enamel in some cases (Pellegrini and Snoeck, 2016; Wood et al., 2021). The carbonate was extracted following the protocol by(De Winter et al., 2016). Extracted carbonate samples were reacted with 99% orthophosphoric acid ($H_3PO_4 + H_4P_2O_7$) in a carbonate preparation device (GasBench II, by ThermoFinnigan) to produce CO_2, which is purified using a series of condensation traps before being led into an isotope-ratio mass spectrometer (MAT253, by ThermoFinnigan) through a dual inlet interface. Stable isotope ratios were calculated from the ratios of CO_2 masses 44, 45 and 46 analysed by the mass spectrometer and converted to delta values with reference to the international Vienna Pee Dee Belemnite (‰VPDB) scale using the standards NBS19, NBS18, CO-8 and LSVEC (IAEA, Vienna, Austria). Stable isotope results were determined to be reproducible with a standard deviation less than 0.2 ‰ based on repeated measurements of Carrara marble powder. To compare our enamel-bound stable oxygen isotope results with modern and Miocene water oxygen isotope values obtained in previous studies, we used the enamel-water conversion formula for large, water-dependent herbivores from (Hoppe, 2006) and we aligned the VSMOW to VPDB scale using the formula in (Coplen et al., 1983), following the methodology in (de Rooij et al., 2022) and (Wooller et al., 2021).

4. Results and interpretation

4.1 Mineralogical characterization of sediments associated with studied molars

The X-ray diffraction analyses on Mid-Miocene soil samples revealed quartz as the main constituent (*ca.* 95%; Table 1). Samples extracted from areas surrounding the teeth (inside and around) show lower abundance of quartz (absent or 21 to 67%; Table 1) accompanied by a significant contribution of iron-rich minerals (goethite, siderite, ilmenite). In contrast, modern sediment samples representing the host substrate of the Lisbon Zoo are composed of approximately equal amounts of quartz and calcite (52 and 48%, respectively; Table 1). Calcite is not significantly present at any sample retrieved from Mid-Miocene materials. Mid-Miocene sediment samples correspond to detrital quartz-grain deposits, cemented into hard iron-rich crusts encasing the studied molars. Such "induration" is common in semi-arid regions because of epidiagenetic processes (*sensu* Staunton and Fairbridge, 2008), typically found in flood plain alluvium, lacustrine and littoral deposits affected by strong seasonality: wet season leads to dissolution and the dry season to capillary action and evaporation (Beauvais and Colin, 1993; Staunton and Fairbridge, 2008). The presence of dolomite and/or gypsum (see Table 1) is also consistent with strong evaporation scenario (Díaz-Hernández et al., 2013). In contrast, the sediments associated with the modern elephant molar show no evidence of such evaporation processes.

Clay mineral fractions also provided clear differences between Mid-Miocene and modern samples (Fig. 3): In ancient samples only illite was detected, whilst the modern sample is also dominated by illite (84%) but also contains a small amount of smectite (16%; Fig. 6). Nevertheless, these differences may be considered as negligible in terms of original composition of the ancient clay assemblage for two reasons: (i) Smectite decays readily under shallow burial conditions (illitization of smectite) as water is expelled from the interlayer space and sheets become more and more organized, leading to a well crystallized illite crystal structure (Kübler and Jaboyedoff, 2000). It is thus plausible that smectite was a part of the initial composition of the clay assemblage of mid-Miocene soils, as seen for the modern soil sample (Fig. 6). (ii) Sediments reflecting a clay mineral composition of 100% illite are highly uncommon (Journet et al., 2014), corroborating the probable illitization of original smectite. Therefore, the original clay mineral assemblage at both sites can be considered similar, but further comparisons are limited, as soil substrate at the Lisbon Zoo may not necessarily reflect local sediment composition (as described in section 2.2).

4.2. Stable carbon and oxygen isotope composition of tooth enamel bioapatite

Mid-Miocene molar samples present $\delta^{13}C$ values between -9.2 and -9.9‰VPDB (mean value ± standard deviation (s.d.) = -9.7 ± 0.3‰VPDB; Fig. 7), in clear contrast with the modern elephant molars, whose values range from -11.9 to -13.2‰VPDB (mean ± s.d.=-12.8 ± 0.3‰VPDB). Differences in $\delta^{18}O$ are also clear, with Mid-Miocene samples clustering between -1.7 and -6.7‰VPDB (mean ± s.d.=-3.5 ± 1.0‰VPDB) and modern samples between -7.9 and -11.1‰VPDB (mean ± s.d.=-8.6 ± 0.7‰VPDB). The extent of diagenetic alteration can be evaluated by assessing the degree of isotopic heterogeneity and/or homogeneity among specimens from a single deposit(Kohn and Cerling, 2002). In this way, the observed clustering of all Mid-Miocene samples against the tight cluster formed by the modern molar samples is taken as evidence of fair preservation of the older molars. This interpretation is further validated by contrast with available literature for coeval materials and (paleo) environmental conditions deduced for the factors controlling the obtained isotopic differences. When compared with previous studies, we find that both our modern and our *Gomphotherium* $\delta^{13}C$ data aligns well with previous $\delta^{13}C$ measurements for these taxa. The $\delta^{18}O$ values measured in *Gomphotherium* for this study are high compared to most literature $\delta^{18}O$ values of the same genus, while our modern elephant $\delta^{18}O$ values are slightly lower than those of other modern and Pleistocene elephants (Figure 7).

4.3 Elemental composition of molar enamel

Semi-quantitative XRF maps highlight the distribution of multiple elements throughout the tooth specimens (see elemental maps in https://doi.org/10.5281/zenodo.14882824). The maps show clear features elevated in the concentrations of elements such as Fe (example in Fig. 5), which indicate patina or encrustation on the outside of the teeth or cracks in the teeth which are enriched in these detrital elements. The cementum cavity and dentine are also enriched in these elements compared to the enamel layers. These areas were avoided as much as possible during line scanning to exclude the influence of these postmortem processes from our interpretation. Outside these clearly diagenetic features, the enamel of the *G. angustidens* specimens studied here is broadly similar to that of the

https://doi.org/10.5194/egusphere-2025-1770
Preprint. Discussion started: 11 June 2025

modern elephant, and to that of previous other modern mammal tooth enamel (De Winter et al., 2016; Kohn, 2008) attesting to its preservation.

A summary of mean elemental values obtained for selected elements (Ca, P, Na, Mg, Sr, S, Si, Fe, Al, K and Mn) based on quantitative XRF line scans is shown in Table 2 and Figure 8. Because of a wide array of expected differences amongst the studied molars (geological age, geographical origin, taxonomic difference), overall discrepancies in absolute values are beyond the scope of this contribution. Yet, due to the potential interaction with surrounding soil and diagenetic incorporation of Si, Fe, Al, K (e.g., Białas et al., 2021; Brügmann et al., 2012), the fact that these elements show no clear enrichment trend when comparing modern with ancient values seems to point towards a fair preservation of the elemental composition of Mid-Miocene molars (see Table 2).

Iron is the only exception, but likely because Miocene molars are encased on iron-rich crusts (section 4.1). If iron oxide encrustation caused elevated Fe in the fossil specimen, such enrichment should be higher on the outside of the molars, a pattern visible in the line scan results (see below) and the XRF maps (see Appendix; https://doi.org/10.5281/zenodo.14882824). In this case, elemental fluctuations observed in phase with Fe are suspect of diagenetic influence and not interpreted in the discussion. In fact, due to eliminate risk of discussing differences in absolute elemental values due to diagenetic alteration, including depletion or enrichment of some elements (Fig. 8 and Table 2), we focus on discussing elemental trends during tooth growth and elemental associations, as these features may enclose (paleo) environmental fluctuations during the growing period (typically <4/5years (Uno et al., 2020).

Elemental associations were obtained by performing Principal Component Analysis (PCA) on Mid-Miocene and modern elemental data (Fig. 9). Details on preliminary data treatment and exploratory analysis are provided in Supplementary File (Figs. S1 to S4). Principle Component Analysis has been shown to help detecting diagenetic signatures in fossil archives, because elements associated with diagenetic alteration (e.g. Mn and Fe in the case of carbonates (Ullmann and Korte, 2015) or rare earth elements, U and Mn and Fe in the case of bioapatite (de Winter et al., 2019; Kohn, 2008; McMillan et al., 2019) tend to cluster into a clearly distinguishable principle axis due to their strong enrichment in altered parts of the fossils (Coimbra et al., 2020). Modern and ancient samples provided very similar PCA loading plots (Fig. 9A and B). Principle Component 1 (PC1) is characterized by an opposing trend of Ca and P concentrations on the one hand against concentrations of Fe, Si, Al, K (with minor contributions of Mn and Sr) on the other. Principle Component 2 (PC2) represents a trend of Ca and P concentrations contrasted to samples with higher Na, Mg and Sr concentrations. Accordingly, lowered Ca and P values are associated to increased abundance of the remaining elements (“closed sum effect”; Fig. 9A and B), but without relation between the groups of elements separated in different components (PC1: Fe, Si, Al, K; PC2: Na, Mg, Sr). Sample distribution along the PCA score plots (Fig. 9C and D) shows a main cluster from which a small number of samples deviate towards higher concentration of Fe, Si, Al, K (negative PC1 values; horizontal axis) and higher concentration of Na, Mg, Sr (positive PC2 values; vertical axis). Because these elemental associations are seen in both modern and ancient samples, diagenetic control on obtained elemental distributions is unlikely (also shown during exploratory data analysis; Supplementary File). The observed cluster distribution suggests that incorporation of Fe, Si, Al, K and Mn occurs only sporadically and may partly highlight incorporation of small fractions of detrital matter on the edges of the line scans where they exit the enamel. In contrast, Na, Mg and Sr incorporation is recurrent throughout the elemental dataset, suggesting consistent variability within the enamel which may be linked to *in vivo* environmental variability recorded in the teeth (see (De Winter et al., 2016).

https://doi.org/10.5194/egusphere-2025-1770
Preprint. Discussion started: 11 June 2025

The variability in concentrations of the statistically most relevant elements from each cluster defined by PCA (Ca, Na, Fe and Si) along molar growth was tested by representing the fluctuations in their abundance along the measured transects (Fig. 10). Along transects in growth direction through modern elephant molars (Fig. 10A), Ca and Na show pronounced fluctuations, which are inversely correlated. This relationship between Ca and Na is only rarely disrupted when Fe and Si concentrations are conspicuously higher, in which case Ca and Na both decrease (Figure 10. The mid-Miocene elemental transects reflect the same trend (Fig. 10B) with an anti-phase pattern of Ca and Na with significant fluctuations within one single transect. Concentrations of Ca and Na jointly decrease in locations where Fe and Si show sharp increases. The evolution of Fe and Na along the transects, which sample the same part of the ontogenetic history in each molar were further compared to evaluate their potential as seasonality archives (Figs. 11, 12 and 13). The resulting comparison shows that both episodic increases in Fe concentration and periodic fluctuations in Ca and Na concentrations in the modern elephant and Miocene *G. angustidens* molars are reproduced along parallel transects in the same tooth.

5. Discussion

5.1 Stable isotope signatures in bioapatite

5.1.1 Feeding preferences derived from $\delta^{13}C$ signature in Mid-Miocene and modern molars

The stable carbon isotope composition ($\delta^{13}C$ value) of body tissue of extant herbivores reflects the type of vegetation (C_3 vs. C_4) they consume. Terrestrial plants may follow three types of metabolic pathways to fix CO_2 from the atmosphere: the C_4, C_3, CAM pathways (Bender, 1971; Ehleringer et al., 1991; Farquhar et al., 1989). The C_3 and C_4 photosynthetic pathways exhibit different $\delta^{13}C$ values, with most C_4 plants (tropical grasses and sedges) containing carbon with an isotopic value between -10‰ and -15‰VPDB and most C_3 plants (most trees, shrubs, or high-latitude grasses) between -22‰ and -35‰VPDB (Bender, 1971; Vogel, 1980). The distinct isotopic composition of C_3 and C_4 plants translates to a distinct isotopic signature in tooth enamel carbonate that can be used as a proxy for browsing (mostly C_3) versus grazing (mostly C_4) diet of animals. The typical range of $\delta^{13}C$ values for these different feeding strategies shown in Fig. 7 to compare with our results were obtained from (Cerling et al., 2003b, 2003a; Cerling and Harris, 1999; Clementz, 2012; Martínez del Rio and Carleton, 2012). Metabolic pathways in an animal increase the $\delta^{13}C$ values by up to 14‰ in the dental enamel apatite relative to plant tissue they consume (Cerling and Harris, 1999; Patnaik et al., 2019). Further, animals feeding in closed canopy forests have a lowered $\delta^{13}C$ composition compared to those feeding in more open woodland environments due to the recycling of respired CO_2 (^{13}C depleted) on the forest floor and low light intensities at ground level that results in more negative $\delta^{13}C$ values in plants (Cerling et al., 2004; Patnaik et al., 2019; van der Merwe and Medina, 1991). For the present study, additional aspects are of relevance. Indeed, $\delta^{13}C$ values in modern elephant molars are expected to be *ca.* 1.5‰ lower relative to Miocene *G. angustidens* values due to a shift in atmospheric $\delta^{13}C$ since the Industrial Revolution and fossil fuel combustion (Cerling et al., 1997b, p. 97; Passey and Cerling, 2002; Tipple et al., 2010).

The range of $\delta^{13}C$ values obtained for Mid-Miocene samples largely overlaps the range commonly reported for Mid to late-Miocene *Gomphotherium* samples from a variety of locations (Fox and Fisher, 2004; Patnaik et al., 2019; Wu et al., 2018); Fig. 7). All reported values plot along the upper extreme range for C_3 consumers (-8 to -12‰VPDB; Fig. 7), indicating that—also in Iberia—these individuals foraged in partially open, possibly arid conditions, favouring woodlands as their preferred habitat. Additionally, lack of evidence pointing towards of mixed-feeding preferences indicates that western Iberian areas of woodland habitat could support these large-bodied herbivores through the Mid-Miocene. In clear contrast, modern elephant $\delta^{13}C$ values obtained in this study as well as from other localities (Ma et al., 2019; Uno et al., 2020); Fig. 7) plot towards lower values (-10 to below -14‰VPDB), within the range of closed canopy forest environments. Regarding the modern samples

https://doi.org/10.5194/egusphere-2025-1770
Preprint. Discussion started: 11 June 2025

used in this study, the obtained result suggests that the animal developed the molar in the wild, prior to transport to its zoo environment.

5.1.2 Hydrological differences between Mid-Miocene and present-day environments

The $\delta^{18}O$ of tooth enamel reflects the $\delta^{18}O$ of ingested water, largely influenced by precipitation, latitude, altitude, aridity, and evaporative processes, as well as physiological/behavioural water conservation factors and metabolic processes of mammals (Kohn, 1996; Kohn et al., 1996, p. 96; Luz et al., 1984). Obligate drinkers, such as elephants, frequently ingest water, which largely reflect rainfall oxygen-isotope composition whilst more drought-tolerant non-obligate drinking mammals (e.g. *Oryx*) are affected by evaporative enrichment of $\delta^{18}O$ values (Ayliffe and Chivas, 1990; Kohn et al., 1996; Levin et al., 2006; Roberts et al., 2018). Concomitantly, environmental temperature changes (e.g., seasonal) lead to the enrichment of the $\delta^{18}O$ signature in the water source in warmer conditions and relative depletion in cooler conditions (Bryant et al., 1996).

The range of $\delta^{18}O$ values obtained for Mid-Miocene molar samples is similar to the high end of the range of $\delta^{18}O$ values measured in North American Mid to Late-Miocene *Gomphotherium* molar samples found in the literature ((Fox and Fisher, 2004); Fig. 7), but significantly higher (less depleted) than values reported for Indian and Asian Mid-Miocene *Gomphotherium* molars ((Białas et al., 2021; Patnaik et al., 2019; Wu et al., 2018); Fig. 7). Investigating the expected $\delta^{18}O$ values of precipitation along these different areas of the globe during the Miocene provides clues to explain these differences. The obtained oxygen isotope values in the Mid-Miocene molar samples overlap almost exactly with $\delta^{18}O$ values modelled for rainfall during dry season in western Iberia during the Middle Miocene (Botsyun et al., 2022). Similarly, oxygen isotope compositions in Asian *Gomphotherium* molars are also compatible with pedogenic carbonate $\delta^{18}O$ values from the Chinese Loess Plateau and northern Pakistan, which record the isotopic value of local surface waters in these Asian region (Quade et al., 1989; Wang et al., 2023, p. 23). Considering this relationship, the comparison between $\delta^{18}O$ values recorded in modern and fossil molars reveals that Mid-Miocene weather in western Iberia was likely warmer and/or less humid than in Asia during coeval times.

Comparing modern elephant enamel $\delta^{18}O$ values and local precipitation values in SW Iberia generates a significant discrepancy of ca. 5‰ (Fig. 7). Such a difference is not observed in other modern samples (Fig. 7), which show a very consistent overlap in $\delta^{18}O$ values between $\delta^{18}O_{enamel}$ and $\delta^{18}O_{precipitation}$. Therefore, as already suspected from the interpretation of $\delta^{13}C$ values, the modern elephant living at the Lisbon Zoo is unlikely to have developed his molar in that locality, thus reflecting $\delta^{18}O$ values of the original location in the wild. Based on considerably depleted $\delta^{18}O$ values (ca. -8.5‰), possible origins of the modern specimen include central Angola, southern Democratic Republic of the Congo or Zambia, where the more depleted range of surface water $\delta^{18}O$ values overlaps with $\delta^{18}O$ values of drinking water expected based on the enamel-$\delta^{18}O$ values in our modern elephant specimen ("Water Isotopes Database," 2023).

In summary, carbon and oxygen-isotope values obtained from Mid-Miocene molar samples demonstrate an open-canopy woodland habitat preference for West Iberian *Gomphotherium*. Local food supply sustained browsing communities even during dry season, as no evidence of grazing was detected in $\delta^{13}C$ values. Therefore, warm and dry conditions seem to have prevailed in Western Iberia during the Mid-Miocene. To isolate seasonal-scale variability in the paleoenvironment, high-resolution elemental data are gathered and interpreted below.

5.2 Elemental associations and chemical variability

5.2.1 Trace element concentrations in tooth enamel

Tooth enamel is regarded as one of the most diagenetically inert biominerals and its chemical and isotopic compositions are preferred paleoenvironmental and paleoclimatic proxies (Forbes et al., 2010; Fricke and O'Neil, 1996; Kohn, 1996; Kohn and Cerling, 2002). During precipitation, enamel biomineral composition not only respond to the local chemical environment, i.e. the bioavailability of chemical elements, but also to physiological and taxonomical characteristics. Therefore, our research design comparing related proboscidean taxa aims to isolate climatic and environmental information from the chemical composition of the bioapatite samples.

The nano- to microcrystalline structure of tooth bioapatite has several sites for cations and anions, which permits the uptake of a variety of elements with rather different chemical features. These elements find their way from the environment into plant and animal tissue, including bone and tooth material. For this reason, the chemical and isotopic composition of bioapatite became an important tool to monitor climatic and ecological change (Kohn and Cerling, 2002; Macfadden et al., 1999; Tütken et al., 2007). The bioapatite mineral lattice can accommodate iso- and heterovalent substitutions during life or diagenesis varying its chemical composition through (geological) time, making bioapatite a unique archive of physical and chemical information for both the living cycle and the events occurring after death (Malferrari et al., 2019).

5.2.2 Differential incorporation of major and trace elements in molar enamel

The inorganic component of mineralized enamel is composed of 89% calcium hydroxyapatite and small amounts of calcium carbonate, calcium fluoride and magnesium phosphate. Biological apatite in enamel (and dentin) are deficient in calcium, rich in carbonates and prone to structural element replacement (LeGeros, 1986). Ionic substitutions of enamel apatite (bioapatite) include Mg^{2+}, Na^{+}, Mn^{2+}, $Ni^{2+,}$ Cu^{2+} or Zn^{2+} for Ca^{2+}; Cl^{-} or F^{-}/CO_3^{2-} for OH^{-}; and HPO_4^{2-}, CO_3^{2-}, AsO_4^{3-}, SO_4^{2-} for PO_4^{3-} (Sakae et al., 1991; Sarna-Boś et al., 2022; Shaik et al., 2021). During lifetime, demineralization and remineralization processes are constantly alternating on the surface of each tooth, also contributing to potential changes in elemental composition of teeth (Nedoklan et al., 2021).

Magnesium is the most abundant Ca-substituting trace element in enamel, essential for the proper development of the tooth structure (Sarna-Boś et al., 2022; Sharma et al., 2021). Magnesium (and sodium) can replace Ca by ion exchange on the crystal surface during the secretion and maturation of primary bioapatite. It may occur in a labile status, probably adsorbed onto the crystal surfaces (Aoba et al., 1992a, 1992b). The elemental association obtained for both modern and ancient proboscidean molars, which clearly show an inverse trend between Ca and P concentrations when compared to abundances of Mg, Na and Sr (Fig. 9A and B), indicates that Ca replacement within enamel crystal surfaces occurred naturally during molar development and/or during remineralization processes during the animal's lifetime. The fact that the largest cluster of samples is responding to this trend (Fig. 9C and D) shows that this process is dominant over time, corresponding to tooth growth and later maintenance stages, and not principally related to post-mortem diagenetic processes.

As observed by other authors, small amounts of externally incorporated elements (Si, Al, and Fe, Mn and rare-earth elements) can also be found in fossil enamel, as long-term preservation of bioapatite involves recrystallization and alteration processes, which drive enrichment of elements not naturally abundant in unaltered enamel (Malferrari et al., 2019). Accordingly, minor enrichment or depletion of key elements near the outer enamel rim may indicate the mobilization of these elements into the bioapatite structure during diagenesis (see Fig. 5 for Fe; (de Winter et al., 2019; Kohn, 2008). Conversely, lack of significant elemental changes in enamel Fe (and Mn) from the outer rim of the tooth towards the innermost sections, as seen in our *Gomphotherium* specimens (see Fig. 11), denotes inefficient impregnation of interstitial Fe- and Mn-oxides and oxyhydroxides (Kohn et al., 1999). Additionally, lack of a clear difference in the elemental distribution between modern to fossil data is typically taken as a good indicator that diagenesis had no significant influence on their distribution (Białas et al., 2021). In conclusion, the following previously established lines of evidence for screening for diagenetic influence on elemental enamel composition led us to conclude that our *G. angustidens* dataset reliably records past dietary and environmental change:

1. Modern and ancient samples show similar elemental associations (Fig. 9A and B) and age-dependent elemental enrichment in Fe, Si and Al is not observed (Table 2);
2. There is no clear pattern of trace element enrichment along the outer rims affecting the locations of the selected transects (Fig. 10);
3. Only a small set of samples (13 and 17% of modern and ancient data; respectively) shows elevated abundance of key elements associated with diagenetic alteration (as isolated in PC1; Fig. 9C and D), showing this to be a sporadic enrichment events, rather than a pervasive process.

Even at early diagenetic stages, local sedimentary factors influencing the mobilization of FeO, F and SO_3, such as rock composition, pH value and redox potential, can control the introduction of these elements into the tooth materials during fossilization. Similarly, comparable concentrations of K_2O, SiO_2, and Al_2O_3 in both modern and fossil materials indicate that crystallization or mechanical introduction of silicate phases into the fossil during diagenesis is of low importance. Therefore, even elements typically attributed to early diagenetic evolution (Fe, Si, Al, K) can be interpreted to reflect *in vivo* processes similar to the distribution of other major to minor elements (e.g., Brügmann et al., 2012). Short-lived periods of significant incorporation of Fe, Si, Al, K are inversely correlated to tooth growth and maintenance processes evidenced by reduced Mg and Na fixation (Figs. 9 and 10). This is taken as evidence of periods of environmental stress.

5.2.2. Elemental abundance in *Gomphotherium* molars reveals geophagic behaviour in ancient proboscideans

The patterns of trace element concentration identified in the XRF line scans through the *Gomphotherium* tooth enamel record differential elemental incorporation during the animal's lifetime. Potential sources of elemental enrichment and causes leading to elemental depletion must be interpreted in the light of natural behaviours carried out in response to environmental conditions (Wheelock, 1980; Białas et al., 2021). Amongst these, geophagy is commonly observed in elephants. Geophagy is defined as the deliberate and regular consumption of earthy materials such as soils, clays or sediments by animals and humans (Abrahams and Parsons, 1996) and functions to supplement dietary mineral deficiencies, alleviate gastrointestinal disorders or detoxify unpalatable foods (Chandrajith et al., 2009; Holdø et al., 2002; Houston et al., 2001; Sach et al., 2019; Wheelock, 1980). Soils consumed by African elephants were previously demonstrated to have higher Na^+ concentrations than the surrounding soils, hence deduced to be used to supplement an inadequate dietary-sodium intake (Chandrajith et al., 2009; Wheelock, 1980). However, other possible roles of soil have also been hypothesized as important in determining the extent of geophagy, including detoxification of plant secondary compounds, countering the effects of acidosis (Houston et al., 2001). Mineral supplementation is most likely not the sole factor driving geophagic behaviour (Holdø et al., 2002).

Further evidence for the relevance of geophagy and local sedimentary contexts in modern elephants is deduced from the fact that soil used by elephants at Ngorongoro (North Tanzania) contains ca. 35% kaolinite (Houston et al., 2001). Kaolinite, through its adsorptive ability, is effective in neutralizing the activity of many plant secondary (toxic) compounds also serving as a barrier to protect the gut lining from toxins in the food (e.g., tannins and alkaloids; Sach et al., 2019). In this way, forest elephants, which have access to kaolin soils, may be able to feed on a wider range of forest plant species, which can be beneficial under nutritional stress resulting from low food quality during dry season (Suba et al., 2016). Elephants purposefully select soils with high proportions of kaolinite and illite, particularly during the dry season when food quality is relatively low (Chandrajith et al., 2009). In this context, the clay assemblage recovered from both modern and ancient materials (Fig. 6), dominated by illite [$KAl_2(Si_3, Al)O_{10}(OH)_2$] and small contribution of smectite [$(Na,Ca)_{0,3}(Al,Fe,Mg)_2$(Si,

https://doi.org/10.5194/egusphere-2025-1770
Preprint. Discussion started: 11 June 2025

$Al)_4O_{10}(OH)_2 \bullet n(H_2O)]$ explains the incorporation of minor elements via geophagic behaviour, providing a viable source of Fe, Si, K, Al (Figs. 9 and 10). Illite is reported to be the most abundant clay mineral in land surfaces at a global scale (Ito and Wagai, 2017).

An alternative hypothesis explaining these spikes in Fe, Si and Al in our trace element profiles could be the incorporation (either *in vivo* or postmortem) of fine-grained sediment into cracks in the enamel. This would not require digestion of the minerals, but, if incorporated *in vivo*, would still point to geophagic behaviour. After closely examining the distribution of these elements in XRF maps (Figure 10 and Appendix; https://doi.org/10.5281/zenodo.14882824) as well as the texture of the enamel at the location of the XRF line scans, we consider this explanation unlikely, as no evidence of cracks in the enamel is found at the measurement locations. This is a result of our measurement strategy, in which we deliberately avoided these cracked areas when programming our XRF profiles (see **section 3.3.2**).

We hypothesize that the short-lived, sporadic increments in Fe, Si, Al in both modern and ancient molars result from elemental incorporation due to geophagic behaviour during stressful, dry season conditions. By comparing Fe trends along all measured transects (Fig. 11), it is possible to identify the occurrence of several dry periods during molar growth (Fig. 11B, D, F and H). It is not possible to confirm their seasonal periodicity with certainty here, as enamel growth rates cannot be independently reconstructed, limiting the estimation of the amount of time comprised in each transect. Tentatively, three to four dry seasons are identified based on the sharp Fe increments coinciding with cyclical patterns in Na, suggesting that the obtained elemental archive recovers a period of 3 to 4 years in the life of these animals. Based on the reasoning above, even small amounts of externally incorporated elements (Fe, Si, Al) can serve as proxies to identify seasonality in modern and ancient molar samples if the animals participated in seasonal geophagy. This result shows that Miocene seasonality was sufficiently pronounced to have an impact on animal behaviour, stimulating geophagic behaviour under seasonally stressful (warm and dry) conditions. Complementing these findings, Na distribution likely indicates variations in tooth growth, with higher Na values highlighting growth under optimal conditions (Fig. 12). The Na record showing smooth long-duration increments along one to three periods (Fig. 12B, D, F and H) supports the interpretation that Na in our *Gomphotherium* can be used as a proxy for seasonal changes in tooth growth rate, while the Fe spikes highlight periods of drought, geophagy and reduced growth. This observation is supported by evidence of Na deficiency as one of the drivers of geophagic behaviour and natural preference for Na-rich sediments (Chandrajith et al., 2009; Wheelock, 1980). The timing of elemental signatures in the trace element records, which reflect dry season, does not overlap with those interpreted to reflect more optimal growth conditions (Fig. 13), which corroborates the usefulness of differential elemental incorporation as indicators of seasonal variability in environmental conditions in ancient teeth. Based on these findings, the applicability of trace elemental concentrations in well-preserved fossil enamel bioapatite as proxies for geophagy behaviour and growth stress during past dry seasons is encouraging.

6. Conclusions

A combination of stable isotope and trace element analyses in molar enamel in Middle Miocene *G. angustidens* from Western Iberia and modern *L. africana* from western Iberia reveals similar responses of tooth bioapatite chemistry to episodic changes in the environment in both taxa. Based on stable carbon and oxygen isotope composition in both taxa, Iberia was characterized by a warm and seasonally dry climate during the Middle Miocene, and that *G. angustidens* thrived in an open-canopy woodland ecosystem in this area. In contrast, the modern *L. africana* specimen developed his molar in a Central African closed-canopy forest environment. Episodic increases in Fe and Si observed in trace element profiles through *G. angustidens* molar enamel hint at geophagy behaviour during seasonally dry and warm periods in this extinct taxon, behaviour patterns, which are also observed in modern *L. africana*. Cross-validation via independent proxies suggests surrounding sediment as a probable source of elemental enrichment, incorporated during molar development and/or during remineralization processes. These results demonstrate the application of high-resolution (sub-seasonal scale) trace element records through fossil teeth is critical to reconstruct the behaviour patterns of extinct mammals in response to climate variability in their living environment.

7. Acknowledgments

RC acknowledges financial support from Geobiotec research Group (UIDB/04035/2020). MR thanks the Stimulus of Scientific Employment, Individual Support – 2018 Call grant by the Fundação para a Ciência e a Tecnologia (Portugal, CEECIND/02199/2018) and GeoBioTec as well as the Fundação para a Ciência e a Tecnologia for the funding of the project 2021 EXPL/CTA-PAL/0832/2021 which directly supports this research. DEL is recipient of a PhD grant funded by Fundação para a Ciência e a Tecnologia (grant number 2020.05395.BD). RM is founded by Fundação para a Ciência e a Tecnologia (grant number 2021.08458.BD). We also thank Micael Martinho and Carla Alexandra Tomás from the preparation laboratory at GEAL-ML as well as Lígia Castro and Eduarda Ferreira from the Earth Sciences Department at FCT-NOVA. Finally, a special thanks to the project manager Marlene Monte from NOVA.ID.FCT. PC thanks Research Foundation Flanders (FWO) for purchasing µXRF and VUB Strategic Research for funding. NdW acknowledges financial support from the Flemish Research Council (FWO postdoctoral fellowship; 12ZB220N and FWO Climate Prize) as well as the Dutch Research Council (NWO) for his VENI fellowship (“MACRO”; VI.Veni.222.354).

Data availability. Supplementary data and figures belonging to this study were stored in the open-source online repository Zenodo (https://doi.org/10.5281/zenodo.14882824)

Author contributions. RC, NdW, and MR conceived the work; all authors wrote, reviewed and edited the manuscript. Samples were collected by MR, RB, DEL, PL and RM; laboratory procedures were supervised and carried out by RC, NdW, MR and AG. FR and PC provided the framework, facilities and necessary support to develop this research.

Competing interest. *Some authors are members of the editorial board of journal Biogeosciences.*

https://doi.org/10.5194/egusphere-2025-1770
Preprint. Discussion started: 11 June 2025

Figure captions

Figure 1. Relevant aspects of Proboscidean morphology and dental anatomy. A) Artistic illustration of *Gomphotherium angustidens* and scale relative to human silhouette (adapted from ("*Gomphotherium angustidens* by cisiopurple on DeviantArt," 2022), ©cisiopurple). B) Schematic representation of molar growth process (adapted from (Jayachandran, 2022) ©Wildlife SOS). C) Molar structure and relative distribution of enamel, dentine and cement (adapted from ("What Did Lupe Eat? - Mammoth Discovery," n.d.) ©Children's Discovery Museum, San Jose, USA). E) Lophodont of elephant in surface view, describing the intricate folding of enamel and dentine to form transverse ridges or lophs (adapted from Bhavya, 2017).

Figure 2. Geographical setting of the studied areas. A) Location of the Portuguese mainland in the Iberia Peninsula. B) Regional distribution of main geological outcrops at the Lisbon area (adapted from LNEG-LGM, 2010). Squares indicate the location of studied sections. C) General biochronostratigraphic scheme for the Miocene and stratigraphic context of studied deposits at the Lisbon area (adapted from Pais et al., 2012). D and E) Field aspect at the localities where the samples were extracted. The molars analysed in this study originate from the Quinta da Farinheira in the Lower Tagus Basin (Areias do Vale de Chelas, Lisbon). The Chelas unit has been designated SDL1 by Antunes & Ginsburg (2003) and Vb by Cotter (1956), with an estimated age of (~15.9–16.1 Ma) and is highlighted by a red arrow. It belongs to the Langhian stage and the MN5 biozone (13.7–16.0 Ma).

Figure 3. General aspect of uncut molar samples. A to C) *Gomphotherium angustidens* molars, note less significant wear of the collected samples from A to C. D) Modern L. Africana molar, showing typical diamond-shaped ridges.

Figure 4. Microscope composite of longitudinally cut modern and Mid-Miocene molar samples with indication of elemental transects chosen for each section (red arrows). Note the inwards-outwards direction of all transects, along growth direction Specimen FCT-DCT 4945 in the top right, FCT-DCT 4933 bottom center and FCT-DCT 4943 on the far right. The modern elephant molar is depicted in the bottom left.

Figure 5. Relative elemental abundance for all specimen, here shown for iron and strontium (distribution of other elements can be found at https://doi.org/10.5281/zenodo.14882824). Note the lack of areas denoting higher iron abundance along selected transects and the clear Sr concentration pattern highlighting well-preserved tooth morphology.

Figure 6. Clay mineral assemblage for Mid-Miocene sediment samples collected from areas adjacent to the molars, around and inside cavities. Modern sediment sample reflects soil substrate from the Lisbon Zoo (see text for details). Note the dominance of illite in all cases, along with minor contribution of smectite for the modern sample.

Figure 7. Biplot representation of stable carbon and oxygen isotope values, highlighting the differences between the two sets of samples tested (modern *vs.* Mid-Miocene). Shaded fields represent C and O isotope values in enamel-bound carbonate reported by other authors (see reference list) for Mid-

https://doi.org/10.5194/egusphere-2025-1770
Preprint. Discussion started: 11 June 2025

Miocene and modern settings. Vertical arrows indicate range of variation of oxygen isotope values representative of rainfall composition at different localities (modern and ancient). Oxygen isotope values of water (right vertical scale) are compared to oxygen isotope values in bioapatite using the formula for large, water-dependent herbivores from (Hoppe, 2006) and we aligned the VSMOW to VPDB scale using the formula in (Coplen et al., 1983) following the methodology in (de Rooij et al., 2022) and (Wooller et al., 2021) . Forest/woodlands range of carbon-isotope variation after Patnaik et al. (2019) and references therein.

Figure 8. Boxplot representation (median and interquartile distance) of absolute elemental concentrations (in ppm). A and B) note similar distribution of Ca and P; C and D) lowered values for ancient samples regarding Na and Mg; E to K) overall higher median values for the remaining proxies (except K). See Table 2 for full elemental range, mean and standard deviation.

Figure 9. Principal component analysis computed for the modern and Mid-Miocene samples. A and B) Principal component loadings explaining 51 to 66% of the total variability of each set of samples. Note similar distribution of elements along the PC axis. Modern Mn and S were not used due to low number of measurements available (N<30%). C and D) Principal component scores indicating sample distribution along the PCA space. Note main clusters of samples in both cases, with only few samples (13% to 16% of the total number of samples) departing from the observed main trend.

Figure 10. Elemental trend of selected proxies (Ca, Na, Fe and Si) for all measured transects (see Figs. 4 and 5 for exact measurement sites). A) Trend lines for modern transects. B) Trend lines for Mid-Miocene transects. Note overall similar records of Ca vs. Na and Fe vs. Si, as well as lack of clear enrichment or depletion trends along each transect. Note opposite variation pattern for Ca and Na, except when Fe and Si become significantly higher (white dashed boxes). Trend lines smoothed (10 points adjacent averaging); numerals according to Figure 4. Colors represent the different enamel transects analyzed. The same color scheme is used consistently across all figures to maintain clarity and allow for easy comparison of the different lines or transects.

Figure 11. Elemental trend line obtained for Fe measurements (line numbers as in Figure 4). A, C E and G) Record of Fe abundance along growth direction (in mm). B, D F and H) Same datasets stacked and slightly adjusted (vertically and horizontally) to compare different transects that represent similar portions of the molar. (*) lines not to scale: mean horizontal scaling factor of 5.1; mean vertical scaling factor of 3.3 (see Table S1 in Appendix). Drawing represents dry season periods. Colors represent the different enamel transects analyzed. The same color scheme is used consistently across all figures to maintain clarity and allow for easy comparison of the different lines or transects.

Figure 12. Elemental trend line obtained for Na measurements (line numbers as in Figure 3). A, C and E) Record of Na abundance along growth direction (in mm). B, D and F) Same datasets stacked and slightly adjusted (vertically and horizontally) to compare different transects that represent similar portions of the molar. (*) lines not to scale: mean horizontal scaling factor of 5.1; mean vertical scaling factor of 1 (see Table S1 in Appendix). Drawing symbol represents wet season periods. Colors represent the different enamel transects analyzed. The same color scheme is used consistently across all figures to maintain clarity and allow for easy comparison of the different lines or transects.

Figure 13. Compilation of elemental trend lines for Fe and Na as shown in Figures 11 and 12. A to C) Mid-Miocene transects in growth direction showing alternating peaks of higher abundance of the chosen elements. D) Modern transects in growth direction showing alternating peaks of higher abundance of the chosen elements.

Table 1. Semiquantitative abundance (%) of bulk mineralogical composition of sediment samples.

Table 2. Mean (±standard deviation; s.d.), minimum and maximum elemental values obtained for selected proxies obtained from Miocene and modern samples.

References

Abrahams, P.W., Parsons, J.A., 1996. Geophagy in the Tropics: A Literature Review. The Geographical Journal 162, 63–72. https://doi.org/10.2307/3060216

Antunes, M.T., Ginsburg, L., 2003. The last Anthracothere Brachyodus onoideus (Mammalia, Artiodactyla) from westernmost Europe and its extinction. Ciências da Terra 15, 161–172.

Antunes, M.T., Pais, J., 1984. Climate during Miocene in Portugal and its evolution. Paléobiologie continentale 14, 75–89.

Aoba, T., Moreno, E.C., Shimoda, S., 1992a. Competitive adsorption of magnesium and calcium ions onto synthetic and biological apatites. Calcif Tissue Int 51, 143–150. https://doi.org/10.1007/BF00298503

Aoba, T., Shimoda, S., Moreno, E.C., 1992b. Labile or surface pools of magnesium, sodium, and potassium in developing porcine enamel mineral. J Dent Res 71, 1826–1831. https://doi.org/10.1177/00220345920710111201

Ayliffe, L.K., Chivas, A.R., 1990. Oxygen isotope composition of the bone phosphate of Australian kangaroos: Potential as a palaeoenvironmental recorder. Geochimica et Cosmochimica Acta 54, 2603–2609. https://doi.org/10.1016/0016-7037(90)90246-H

Ayliffe, L.K., Lister, A.M., Chivas, A.R., 1992. The preservation of glacial-interglacial climatic signatures in the oxygen isotopes of elephant skeletal phosphate. Palaeogeography, Palaeoclimatology, Palaeoecology 99, 179–191. https://doi.org/10.1016/0031-0182(92)90014-V

Beauvais, A., Colin, F., 1993. Formation and transformation processes of iron duricrust systems in tropical humid environment. Chemical Geology 106, 77–101. https://doi.org/10.1016/0009-2541(93)90167-H

Bender, M.M., 1971. Variations in the 13C/12C ratios of plants in relation to the pathway of photosynthetic carbon dioxide fixation. Phytochemistry 10, 1239–1244. https://doi.org/10.1016/S0031-9422(00)84324-1

Bhavya, S., 2017. 3 Main Types of Teeth Found in Mammals | Vertebrates | Chordata | Zoology. Zoology Notes. URL https://www.notesonzoology.com/mammals/3-main-types-of-teeth-found-in-mammals-vertebrates-chordata-zoology/8495 (accessed 1.10.24).

Białas, N., Prymak, O., Singh, N.P., Paul, D., Patnaik, R., Epple, M., 2021. Teeth of Past and Present Elephants: Microstructure and Composition of Enamel in Fossilized Proboscidean Molars and Implications for Diagenesis. Geochemistry, Geophysics, Geosystems 22, e2020GC009557. https://doi.org/10.1029/2020GC009557

Blaise, E., Balasse, M., 2011. Seasonality and season of birth of modern and late Neolithic sheep from south-eastern France using tooth enamel δ 18 O analysis. Journal of archaeological Science 38, 3085–3093.

Botsyun, S., Ehlers, T.A., Koptev, A., Böhme, M., Methner, K., Risi, C., Stepanek, C., Mutz, S.G., Werner, M., Boateng, D., Mulch, A., 2022. Middle Miocene Climate and Stable Oxygen Isotopes in Europe Based on Numerical Modeling. Paleoceanography and Paleoclimatology 37, e2022PA004442. https://doi.org/10.1029/2022PA004442

Brown, G., Brindley, G.W., 1980. X-ray Diffraction Procedures for Clay Mineral Identification, in: Brindley, G.W., Brown, G. (Eds.), Crystal Structures of Clay Minerals and Their X-Ray Identification. Mineralogical Society of Great Britain and Ireland, p. 0. https://doi.org/10.1180/mono-5.5

Brügmann, G., Krause, J., Brachert, T.C., Stoll, B., Weis, U., Kullmer, O., Ssemmanda, I., Mertz, D.F., 2012. Chemical composition of modern and fossil hippopotamid teeth and implications for paleoenvironmental reconstructions and enamel formation – Part 2: Alkaline earth elements as tracers of watershed hydrochemistry and provenance. Biogeosciences 9, 4803–4817. https://doi.org/10.5194/bg-9-4803-2012

Bryant, J.D., Froelich, P.N., Showers, W.J., Genna, B.J., 1996. Biologic and climatic signals in the oxygen isotopic composition of Eocene-Oligocene equid enamel phosphate. Palaeogeography, Palaeoclimatology, Palaeoecology, Biogenic Phosphates as Palaeoenvironmental Indicators 126, 75–89. https://doi.org/10.1016/S0031-0182(96)00071-5

Burls, N.J., Bradshaw, C.D., De Boer, A.M., Herold, N., Huber, M., Pound, M., Donnadieu, Y., Farnsworth, A., Frigola, A., Gasson, E., von der Heydt, A.S., Hutchinson, D.K., Knorr, G., Lawrence, K.T., Lear, C.H., Li, X., Lohmann, G., Lunt, D.J., Marzocchi, A., Prange, M., Riihimaki, C.A., Sarr, A.-C., Siler, N., Zhang, Z., 2021. Simulating Miocene Warmth: Insights From an Opportunistic Multi-Model Ensemble (MioMIP1). Paleoceanography and Paleoclimatology 36, e2020PA004054. https://doi.org/10.1029/2020PA004054

Cantalapiedra, J.L., Sanisidro, Ó., Zhang, H., Alberdi, M.T., Prado, J.L., Blanco, F., Saarinen, J., 2021. The rise and fall of proboscidean ecological diversity. Nat Ecol Evol 5, 1266–1272. https://doi.org/10.1038/s41559-021-01498-w

Cerling, T.E., Harris, J.M., 1999. Carbon isotope fractionation between diet and bioapatite in ungulate mammals and implications for ecological and paleoecological studies. Oecologia 120, 347–363.

Cerling, T.E., Harris, J.M., Ambrose, S.H., Leakey, M.G., Solounias, N., 1997a. Dietary and environmental reconstruction with stable isotope analyses of herbivore tooth enamel from the Miocene locality of Fort Ternan, Kenya. Journal of Human Evolution 33, 635–650.

Cerling, T.E., Harris, J.M., Leakey, M.G., 2003a. 12.2. Isotope Paleoecology of the Nawata and Nachukui Formations at Lothagam, Turkana Basin, Kenya, in: 12.2. Isotope Paleoecology of the Nawata and Nachukui Formations at Lothagam, Turkana Basin, Kenya. Columbia University Press, pp. 605–624. https://doi.org/10.7312/leak11870-024

Cerling, T.E., Harris, J.M., Leakey, M.G., Mudida, N., 2003b. 12.1. Stable Isotope Ecology of Northern Kenya, with Emphasis on the Turkana Basin, in: 12.1. Stable Isotope Ecology of Northern Kenya, with Emphasis on the Turkana Basin. Columbia University Press, pp. 583–604. https://doi.org/10.7312/leak11870-023

Cerling, T.E., Harris, J.M., MacFadden, B.J., Leakey, M.G., Quade, J., Eisenmann, V., Ehleringer, J.R., 1997b. Global vegetation change through the Miocene/Pliocene boundary. Nature 389, 153.

Cerling, T.E., Hart, J.A., Hart, T.B., 2004. Stable isotope ecology in the Ituri Forest. Oecologia 138, 5–12. https://doi.org/10.1007/s00442-003-1375-4

Chandrajith, R., Kudavidanage, E., Tobschall, H.J., Dissanayake, C.B., 2009. Geochemical and mineralogical characteristics of elephant geophagic soils in Udawalawe National Park, Sri Lanka. Environ Geochem Health 31, 391–400. https://doi.org/10.1007/s10653-008-9178-5

Clementz, M.T., 2012. New insight from old bones: stable isotope analysis of fossil mammals. Journal of Mammalogy 93, 368–380. https://doi.org/10.1644/11-MAMM-S-179.1

Coimbra, R., Huck, S., de Winter, N.J., Heimhofer, U., Claeys, P., 2020. Improving the detection of shell alteration: Implications for sclerochronology. Palaeogeography, Palaeoclimatology, Palaeoecology 559, 109968. https://doi.org/10.1016/j.palaeo.2020.109968

Coplen, T.B., Kendall, C., Hopple, J., 1983. Comparison of stable isotope reference samples. Nature 302, 236–238. https://doi.org/10.1038/302236a0

de Rooij, J., van der Lubbe, J.H.J.L., Verdegaal, S., Hulscher, M., Tooms, D., Kaskes, P., Verhage, O., Portanger, L., Schulp, A.S., 2022. Stable isotope record of *Triceratops* from a mass accumulation (Lance Formation, Wyoming, USA) provides insights into *Triceratops* behaviour and ecology. Palaeogeography, Palaeoclimatology, Palaeoecology 607, 111274. https://doi.org/10.1016/j.palaeo.2022.111274

de Winter, N., Sinnesael, M., Makarona, C., Vansteenberge, S., Claeys, P., 2017. Trace element analyses of carbonates using portable and micro-X-ray fluorescence: Performance and optimization of measurement parameters and strategies. Journal of Analytical Atomic Spectrometry. https://doi.org/10.1039/c6ja00361c

De Winter, N., Snoeck, C., Claeys, P., 2016. Seasonal cyclicity in trace elements and stable isotopes of modern horse enamel. PLoS ONE 11, 1. https://doi.org/10.1371/journal.pone.0166678

de Winter, N.J., Claeys, P., 2016. Micro X-ray fluorescence (µXRF) line scanning on Cretaceous rudist bivalves: A new method for reproducible trace element profiles in bivalve calcite. Sedimentology 64, 231–251. https://doi.org/10.1111/sed.12299

de Winter, N.J., Snoeck, C., Schulting, R., Fernández-Crespo, T., Claeys, P., 2019. High-resolution trace element distributions and models of trace element diffusion in enamel of Late Neolithic/Early Chalcolithic human molars from the Rioja Alavesa region (north-central Spain) help to separate biogenic from diagenetic trends. Palaeogeography, Palaeoclimatology, Palaeoecology 532, 109260. https://doi.org/10.1016/j.palaeo.2019.109260

Díaz-Hernández, J.L., Sánchez-Navas, A., Reyes, E., 2013. Isotopic evidence for dolomite formation in soils. Chemical Geology 347, 20–33. https://doi.org/10.1016/j.chemgeo.2013.03.018

Dirks, W., Bromage, T.G., Agenbroad, L.D., 2012. The duration and rate of molar plate formation in *Palaeoloxodon cypriotes* and *Mammuthus columbi* from dental histology. Quaternary International, Mammoths and Their Relatives 1: Biotopes, Evolution and Human Impact V International Conference, Le Puy-en-Velay, 2010 255, 79–85. https://doi.org/10.1016/j.quaint.2011.11.002

Domingo, L., Cuevas-González, J., Grimes, S.T., Fernández, M.H., López-Martínez, N., 2009. Multiproxy reconstruction of the palaeoclimate and palaeoenvironment of the Middle Miocene Somosaguas site (Madrid, Spain) using herbivore dental enamel. Palaeogeography, Palaeoclimatology, Palaeoecology 272, 53–68.

Ehleringer, J.R., Sage, R.F., Flanagan, L.B., Pearcy, R.W., 1991. Climate change and the evolution of C4 photosynthesis. Trends in Ecology & Evolution 6, 95–99. https://doi.org/10.1016/0169-5347(91)90183-X

Esker, D., Forman, S.L., Widga, C., Walker, J.D., Andrew, J.E., 2019. Home range of the Columbian mammoths (Mammuthus columbi) and grazing herbivores from the Waco Mammoth National Monument, (Texas, USA) based on strontium isotope ratios from tooth enamel bioapatite. Palaeogeography, Palaeoclimatology, Palaeoecology 534, 109291. https://doi.org/10.1016/j.palaeo.2019.109291

Farquhar, G.D., Ehleringer, J.R., Hubick, K.T., 1989. Carbon isotope discrimination and photosynthesis. Annual review of plant biology 40, 503–537.

Forbes, M.S., Kohn, M.J., Bestland, E.A., Wells, R.T., 2010. Late Pleistocene environmental change interpreted from δ13C and δ18O of tooth enamel from the Black Creek Swamp Megafauna site, Kangaroo Island, South Australia. Palaeogeography, Palaeoclimatology, Palaeoecology 291, 319–327. https://doi.org/10.1016/j.palaeo.2010.03.003

Fox, D.L., Fisher, D.C., 2004. Dietary reconstruction of Miocene Gomphotherium (Mammalia, Proboscidea) from the Great Plains region, USA, based on the carbon isotope composition of tusk and molar enamel. Palaeogeography, Palaeoclimatology, Palaeoecology, Incremental Growth in Vertebrate Skeletal Tissues: Paleobiological and Paleoenvironmental Implications 206, 311–335. https://doi.org/10.1016/j.palaeo.2004.01.010

Fricke, H.C., O'Neil, J.R., 1996. Inter- and intra-tooth variation in the oxygen isotope composition of mammalian tooth enamel phosphate: implications for palaeoclimatological and palaeobiological research. Palaeogeography, Palaeoclimatology, Palaeoecology, Biogenic Phosphates as Palaeoenvironmental Indicators 126, 91–99. https://doi.org/10.1016/S0031-0182(96)00072-7

Galhano, C., Rocha, F., Gomes, C., 1999. Geostatistical analysis of the influence of textural, mineralogical and geochemical parameters on the geotechnical behaviour of the 'Argilas de Aveiro' Formation (Portugal). Clay Minerals 34, 109–116. https://doi.org/10.1180/000985599545966

Geraads, D., Zouhri, S., Markov, G.N., 2019. The first Tetralophodon (Mammalia, Proboscidea) cranium from Africa. Journal of Vertebrate Paleontology 39, e1632321. https://doi.org/10.1080/02724634.2019.1632321

Goldner, A., Herold, N., Huber, M., 2014. The challenge of simulating the warmth of the mid-Miocene climatic optimum in CESM1. Climate of the Past 10, 523–536. https://doi.org/10.5194/cp-10-523-2014

Gomphotherium angustidens by cisiopurple on DeviantArt [WWW Document], 2022. URL https://www.deviantart.com/cisiopurple/art/Gomphotherium-angustidens-916106115 (accessed 1.10.24).

Harzhauser, M., Kroh, A., Mandic, O., Piller, W.E., Göhlich, U., Reuter, M., Berning, B., 2007. Biogeographic responses to geodynamics: A key study all around the Oligo–Miocene Tethyan Seaway. Zoologischer Anzeiger - A Journal of Comparative Zoology, Special Issue: Phylogenetic Symposium 246, 241–256. https://doi.org/10.1016/j.jcz.2007.05.001

Harzhauser, M., Piller, W.E., Müllegger, S., Grunert, P., Micheels, A., 2011. Changing seasonality patterns in Central Europe from Miocene Climate Optimum to Miocene Climate Transition deduced from the Crassostrea isotope archive. Global and Planetary Change 76, 77–84. https://doi.org/10.1016/j.gloplacha.2010.12.003

Holbourn, A., Kuhnt, W., Kochhann, K.G.D., Andersen, N., Sebastian Meier, K.J., 2015. Global perturbation of the carbon cycle at the onset of the Miocene Climatic Optimum. Geology 43, 123–126. https://doi.org/10.1130/G36317.1

Holdø, R.M., Dudley, J.P., McDowell, L.R., 2002. Geophagy in the African Elephant in Relation to Availability of Dietary Sodium. Journal of Mammalogy 83, 652–664. https://doi.org/10.1644/1545-1542(2002)083<0652:GITAEI>2.0.CO;2

Hoppe, K.A., 2006. Correlation between the oxygen isotope ratio of North American bison teeth and local waters: Implication for paleoclimatic reconstructions. Earth and Planetary Science Letters 244, 408–417. https://doi.org/10.1016/j.epsl.2006.01.062

Houston, D.C., Gilardi, J.D., Hall, A.J., 2001. Soil consumption by Elephants might help to minimize the toxic effects of plant secondary compounds in forest browse. Mammal Review 31, 249–254. https://doi.org/10.1111/j.1365-2907.2001.00091.x

Iannucci, A., Sardella, R., 2023. What Does the "Elephant-Equus" Event Mean Today? Reflections on Mammal Dispersal Events around the Pliocene-Pleistocene Boundary and the Flexible Ambiguity of Biochronology. Quaternary 6, 16. https://doi.org/10.3390/quat6010016

IPCC, 2023. SYNTHESIS REPORT OF THE IPCC SIXTH ASSESSMENT REPORT (AR6). Intergovernmental Panel on Climate Change, Geneva, Switzerland.

Ito, A., Wagai, R., 2017. Global distribution of clay-size minerals on land surface for biogeochemical and climatological studies. Sci Data 4, 170103. https://doi.org/10.1038/sdata.2017.103

Jayachandran, M., 2022. The Role of Molar Teeth In Age Determination of Elephants [WWW Document]. Wildlife SOS. URL https://wildlifesos.org/elephant/the-role-of-molar-teeth-in-age-determination-of-elephants/ (accessed 1.10.24).

Journet, E., Balkanski, Y., Harrison, S.P., 2014. A new data set of soil mineralogy for dust-cycle modeling. Atmospheric Chemistry and Physics 14, 3801–3816. https://doi.org/10.5194/acp-14-3801-2014

Koch, P.L., Michener, R., Lajtha, K., 2007. Isotopic study of the biology of modern and fossil vertebrates. Stable isotopes in ecology and environmental science 2, 99–154.

Kohn, M.J., 2008. Models of diffusion-limited uptake of trace elements in fossils and rates of fossilization. Geochimica et Cosmochimica Acta 72, 3758–3770. https://doi.org/10.1016/j.gca.2008.05.045

Kohn, M.J., 1996. Predicting animal δ18O: Accounting for diet and physiological adaptation. Geochimica et Cosmochimica Acta 60, 4811–4829. https://doi.org/10.1016/S0016-7037(96)00240-2

Kohn, M.J., Cerling, T.E., 2002. Stable Isotope Compositions of Biological Apatite. Reviews in Mineralogy and Geochemistry 48, 455–488. https://doi.org/10.2138/rmg.2002.48.12

Kohn, M.J., Schoeninger, M.J., Barker, W.W., 1999. Altered states: effects of diagenesis on fossil tooth chemistry. Geochimica et Cosmochimica Acta 63, 2737–2747.

Kohn, M.J., Schoeninger, M.J., Valley, J.W., 1996. Herbivore tooth oxygen isotope compositions: Effects of diet and physiology. Geochimica et Cosmochimica Acta 60, 3889–3896. https://doi.org/10.1016/0016-7037(96)00248-7

Kowalik, N., Anczkiewicz, R., Müller, W., Spötl, C., Bondioli, L., Nava, A., Wojtal, P., Wilczyński, J., Koziarska, M., Matyszczak, M., 2023. Revealing seasonal woolly mammoth migration with spatially-resolved trace element, Sr and O isotopic records of molar enamel. Quaternary Science Reviews 306, 108036. https://doi.org/10.1016/j.quascirev.2023.108036

Kübler, B., Jaboyedoff, M., 2000. Illite crystallinity. Comptes Rendus de l’Académie des Sciences - Series IIA - Earth and Planetary Science 331, 75–89. https://doi.org/10.1016/S1251-8050(00)01395-1

Larramendi, A., 2015. Shoulder Height, Body Mass, and Shape of Proboscideans. acpp 61, 537–574. https://doi.org/10.4202/app.00136.2014

Lee, P.C., Sayialel, S., Lindsay, W.K., Moss, C.J., 2012. African elephant age determination from teeth: validation from known individuals. African Journal of Ecology 50, 9–20. https://doi.org/10.1111/j.1365-2028.2011.01286.x

Lee-Thorp, J., Sponheimer, M., 2003. Three case studies used to reassess the reliability of fossil bone and enamel isotope signals for paleodietary studies. Journal of Anthropological Archaeology 22, 208–216.

LeGeros, R.Z., 1986. Variability of HAP/b-TCP ratios in sintered apatites, in: Journal of Dental Research. AMER ASSOC DENTAL RESEARCH 1619 DUKE ST, ALEXANDRIA, VA 22314, pp. 292–292.

Levin, N.E., Cerling, T.E., Passey, B.H., Harris, J.M., Ehleringer, J.R., 2006. A stable isotope aridity index for terrestrial environments. Proceedings of the National Academy of Sciences 103, 11201–11205. https://doi.org/10.1073/pnas.0604719103

Li, C., Deng, T., Wang, Y., Sun, F., Wolff, B., Jiangzuo, Q., Ma, J., Xing, L., Fu, J., Zhang, J., Wang, S.-Q., 2023. Longer mandible or nose? Co-evolution of feeding organs in early elephantiforms. eLife 12. https://doi.org/10.7554/eLife.90908.1

Liu, A.G.S.C., Seiffert, E.R., Simons, E.L., 2008. Stable isotope evidence for an amphibious phase in early proboscidean evolution. Proceedings of the National Academy of Sciences 105, 5786–5791. https://doi.org/10.1073/pnas.0800884105

Luz, B., Kolodny, Y., Horowitz, M., 1984. Fractionation of oxygen isotopes between mammalian bone-phosphate and environmental drinking water. Geochimica et Cosmochimica Acta 48, 1689–1693.

Ma, J., Wang, Y., Jin, C., Hu, Y., Bocherens, H., 2019. Ecological flexibility and differential survival of Pleistocene Stegodon orientalis and Elephas maximus in mainland southeast Asia revealed by stable isotope (C, O) analysis. Quaternary Science Reviews 212, 33–44. https://doi.org/10.1016/j.quascirev.2019.03.021

Macfadden, B.J., Cerling, T.E., Harris, J.M., Prado, J., 1999. Ancient Latitudinal Gradients of C3/C4 Grasses Interpreted from Stable Isotopes of New World Pleistocene Horse (Equus) Teeth. Global Ecology and Biogeography 8, 137–149.

MacFadden, B.J., Morgan, G.S., Jones, D.S., Rincon, A.F., 2015. Gomphothere proboscidean (Gomphotherium) from the late Neogene of Panama. Journal of Paleontology 89, 360–365. https://doi.org/10.1017/jpa.2014.31

Malferrari, D., Ferretti, A., Mascia, M.T., Savioli, M., Medici, L., 2019. How Much Can We Trust Major Element Quantification in Bioapatite Investigation? ACS Omega 4, 17814–17822. https://doi.org/10.1021/acsomega.9b02426

Martínez del Rio, C., Carleton, S.A., 2012. How fast and how faithful: the dynamics of isotopic incorporation into animal tissues. Journal of Mammalogy 93, 353–359. https://doi.org/10.1644/11-MAMM-S-165.1

McMillan, R., Snoeck, C., de Winter, N.J., Claeys, P., Weis, D., 2019. Evaluating the impact of acetic acid chemical pre-treatment on 'old' and cremated bone with the 'Perio-spot' technique and 'Perios-endos' profiles. Palaeogeography, Palaeoclimatology, Palaeoecology. https://doi.org/10.1016/j.palaeo.2019.05.019

Meckler, A.N., Sexton, P.F., Piasecki, A.M., Leutert, T.J., Marquardt, J., Ziegler, M., Agterhuis, T., Lourens, L.J., Rae, J.W.B., Barnet, J., Tripati, A., Bernasconi, S.M., 2022. Cenozoic evolution of deep ocean temperature from clumped isotope thermometry. Science 377, 86–90. https://doi.org/10.1126/science.abk0604

Meinshausen, M., Nicholls, Z.R.J., Lewis, J., Gidden, M.J., Vogel, E., Freund, M., Beyerle, U., Gessner, C., Nauels, A., Bauer, N., Canadell, J.G., Daniel, J.S., John, A., Krummel, P.B., Luderer, G., Meinshausen, N., Montzka, S.A., Rayner, P.J., Reimann, S., Smith, S.J., van den Berg, M., Velders, G.J.M., Vollmer, M.K., Wang, R.H.J., 2020. The shared socio-economic pathway (SSP) greenhouse gas concentrations and their extensions to 2500. Geoscientific Model Development 13, 3571–3605. https://doi.org/10.5194/gmd-13-3571-2020

Mellinger, M., 1979. Quantitative X-ray diffraction analysis of clay minerals: an evaluation. Saskatchewan Research Council.

Metcalfe, J.Z., Longstaffe, F.J., 2012. Mammoth tooth enamel growth rates inferred from stable isotope analysis and histology. Quaternary Research 77, 424–432. https://doi.org/10.1016/j.yqres.2012.02.002

Methner, K., Campani, M., Fiebig, J., Löffler, N., Kempf, O., Mulch, A., 2020. Middle Miocene long-term continental temperature change in and out of pace with marine climate records. Sci Rep 10, 7989. https://doi.org/10.1038/s41598-020-64743-5

Mothé, D., Ferretti, M.P., Avilla, L.S., 2016. The Dance of Tusks: Rediscovery of Lower Incisors in the Pan-American Proboscidean Cuvieronius hyodon Revises Incisor Evolution in Elephantimorpha. PLoS One 11, e0147009. https://doi.org/10.1371/journal.pone.0147009

Nedoklan, S., Knezovic, Z., Knezovic, N., Sutlovic, D., 2021. NUTRITION AND MINERAL CONTENT IN HUMAN TEETH THROUGH THE CENTURIES. Archives of Oral Biology 124, 105075. https://doi.org/10.1016/j.archoralbio.2021.105075

Oliveira, A., Rocha, F., Rodrigues, A., Jouanneau, J., Dias, A., Weber, O., Gomes, C., 2002. Clay minerals from the sedimentary cover from the Northwest Iberian shelf. Progress in Oceanography, Benthic processes and dynamics at the NW Iberian Margin: resultss of the OMEX II Program 52, 233–247. https://doi.org/10.1016/S0079-6611(02)00008-3

Pais, J., Cunha, P.P., Pereira, D., Legoinha, P., Dias, R., Moura, D., da Silveira, A.B., Kullberg, J.C., González-Delgado, J.A., 2012. The Paleogene and Neogene of Western Iberia (Portugal): A Cenozoic Record in the European Atlantic Domain, in: Pais, J. (Ed.), The Paleogene and Neogene of Western Iberia (Portugal): A Cenozoic Record in the European Atlantic Domain, SpringerBriefs in Earth Sciences. Springer, Berlin, Heidelberg, pp. 1–138. https://doi.org/10.1007/978-3-642-22401-0_1

Passey, B.H., Cerling, T.E., 2002. Tooth enamel mineralization in ungulates: implications for recovering a primary isotopic time-series. Geochimica et Cosmochimica Acta 66, 3225–3234.

Patnaik, R., Singh, N.P., Paul, D., Sukumar, R., 2019. Dietary and habitat shifts in relation to climate of Neogene-Quaternary proboscideans and associated mammals of the Indian subcontinent. Quaternary Science Reviews 224, 105968. https://doi.org/10.1016/j.quascirev.2019.105968

Pellegrini, M., Snoeck, C., 2016. Comparing bioapatite carbonate pre-treatments for isotopic measurements: Part 2—Impact on carbon and oxygen isotope compositions. Chemical Geology 420, 88–96.

Quade, J., Cerling, T.E., Bowman, J.R., 1989. Development of Asian monsoon revealed by marked ecological shift during the latest Miocene in northern Pakistan. Nature 342, 163–166. https://doi.org/10.1038/342163a0

Roberts, P., Stewart, M., Alagaili, A.N., Breeze, P., Candy, I., Drake, N., Groucutt, H.S., Scerri, E.M.L., Lee-Thorp, J., Louys, J., Zalmout, I.S., Al-Mufarreh, Y.S.A., Zech, J., Alsharekh, A.M., al Omari, A., Boivin, N., Petraglia, M., 2018. Fossil herbivore stable isotopes reveal middle Pleistocene hominin palaeoenvironment in 'Green Arabia.' Nat Ecol Evol 2, 1871–1878. https://doi.org/10.1038/s41559-018-0698-9

Sach, F., Dierenfeld, E.S., Langley-Evans, S.C., Watts, M.J., Yon, L., 2019. African savanna elephants (Loxodonta africana) as an example of a herbivore making movement choices based on nutritional needs. PeerJ 7, e6260. https://doi.org/10.7717/peerj.6260

Saegusa, H., Nakaya, H., Kunimatsu, Y., Nakatsukasa, M., Tsujikawa, H., Sawada, Y., Saneyoshi, M., Sakai, T., 2014. Earliest elephantid remains from the Late Miocene locality, Nakali, Kenya, in: Abstract Book of the VIth International Conference on Mammoths and Their Relatives. Scientific Annals of the School of Geology, Special. p. 175.

Sakae, T., Mishima, H., Kozawa, Y., 1991. Proboscidea Fossil Teeth Suggest the Evolution of Enamel Crystals, in: Suga, S., Nakahara, H. (Eds.), Mechanisms and Phylogeny of Mineralization in Biological Systems. Springer Japan, Tokyo, pp. 477–481. https://doi.org/10.1007/978-4-431-68132-8_76

Sarna-Boś, K., Boguta, P., Skic, K., Wiącek, D., Maksymiuk, P., Sobieszczański, J., Chałas, R., 2022. Physicochemical Properties and Surface Characteristics of Ground Human Teeth. Molecules 27, 5852. https://doi.org/10.3390/molecules27185852

Schultz, L.G., 1964. Quantitative interpretation of mineralogical composition from X-ray and chemical data for the Pierre Shale. U.S. Geological Survey Professional Papers 391–C.

Shaik, I., Dasari, B., Shaik, A., Doos, M., Kolli, H., Rana, D., Tiwari, R.V.C., 2021. Functional Role of Inorganic Trace Elements on Enamel and Dentin Formation: A Review. J Pharm Bioallied Sci 13, S952–S956. https://doi.org/10.4103/jpbs.jpbs_392_21

Sharma, V., Srinivasan, A., Nikolajeff, F., Kumar, S., 2021. Biomineralization process in hard tissues: The interaction complexity within protein and inorganic counterparts. Acta Biomaterialia, Biomineralization: From Cells to Biomaterials 120, 20–37. https://doi.org/10.1016/j.actbio.2020.04.049

Staunton, S., Fairbridge, R.W., 2008. Duricrusts and Induration, in: Chesworth, W. (Ed.), Encyclopedia of Soil Science, Encyclopedia of Earth Sciences Series. Springer Netherlands, Dordrecht, pp. 192–198. https://doi.org/10.1007/978-1-4020-3995-9_168

Steinthorsdottir, M., Coxall, H.K., Boer, A.M. de, Huber, M., Barbolini, N., Bradshaw, C.D., Burls, N.J., Feakins, S.J., Gasson, E., Henderiks, J., Holbourn, A., Kiel, S., Kohn, M.J., Knorr, G., Kürschner, W.M., Lear, C.H., Liebrand, D., Lunt, D.J., Mörs, T., Pearson, P.N., Pound, M.J., Stoll, H., Strömberg, C. a. E., 2020. The Miocene: the Future of the Past. Paleoceanography and Paleoclimatology n/a, e2020PA004037. https://doi.org/10.1029/2020PA004037

Suba, R.B., Beveridge, N.G., de Iongh, H.H., de Snoo, G.R., 2016. Bornean elephant food preference based on Nuclear Magnetic Resonance (NMR) metabolic profiling techniques.

Super, J.R., Thomas, E., Pagani, M., Huber, M., O'Brien, C., Hull, P.M., 2018. North Atlantic temperature and pCO2 coupling in the early-middle Miocene. Geology 46, 519–522. https://doi.org/10.1130/G40228.1

Thorez, J., 1976. Practical identification of clay minerals: A handbook for teachers and students in clay mineralogy. Dison, Belgique.

Tipple, B.J., Meyers, S.R., Pagani, M., 2010. Carbon isotope ratio of Cenozoic CO2: A comparative evaluation of available geochemical proxies. Paleoceanography 25. https://doi.org/10.1029/2009PA001851

Tütken, T., Furrer, H., Walter Vennemann, T., 2007. Stable isotope compositions of mammoth teeth from Niederweningen, Switzerland: Implications for the Late Pleistocene climate, environment, and diet. Quaternary International, From the Swiss Alps to the Crimean

Mountains - Alpine Quaternary stratigraphy in a European context 164–165, 139–150. https://doi.org/10.1016/j.quaint.2006.09.004

Ullmann, C.V., Korte, C., 2015. Diagenetic alteration in low-Mg calcite from macrofossils: a review. Geological Quarterly 59, 3–20, doi: 10.7306/gq.1217. https://doi.org/10.7306/gq.1217

Uno, K.T., Fisher, D.C., Wittemyer, G., Douglas-Hamilton, I., Carpenter, N., Omondi, P., Cerling, T.E., 2020. Forward and inverse methods for extracting climate and diet information from stable isotope profiles in proboscidean molars. Quaternary International, High resolution analyses of large mammals dental remains: broadening horizons 557, 92–109. https://doi.org/10.1016/j.quaint.2020.06.030

van der Merwe, N.J., Medina, E., 1991. The canopy effect, carbon isotope ratios and foodwebs in amazonia. Journal of Archaeological Science 18, 249–259. https://doi.org/10.1016/0305-4403(91)90064-V

Vansteenberge, S., de Winter, N.J., Sinnesael, M., Xueqin, Z., Verheyden, S., Claeys, P., 2020. Benchtop µXRF as a tool for speleothem trace elemental analysis: Validation, limitations and application on an Eemian to early Weichselian (125–97 ka) stalagmite from Belgium. Palaeogeography, Palaeoclimatology, Palaeoecology 538, 109460. https://doi.org/10.1016/j.palaeo.2019.109460

Vogel, J.C., 1980. Fractionation of the Carbon Isotopes During Photosynthesis. Springer Science & Business Media.

Wang, J., Zhou, X., Wang, S., Xu, H., Behling, H., Ye, J., Zheng, Y., Liu, J., Wu, Y., Zhao, K., Zhang, R., Li, X., 2023. C4 expansion of Central Asia in the middle Miocene linked to the strengthening Indian monsoon. Global and Planetary Change 224, 104096. https://doi.org/10.1016/j.gloplacha.2023.104096

Wang, S.-Q., Li, Y., Duangkrayom, J., Yang, X.-W., He, W., Chen, S.-Q., 2017. A new species of *Gomphotherium* (Proboscidea, Mammalia) from China and the evolution of *Gomphotherium* in Eurasia. Journal of Vertebrate Paleontology 37, e1318284. https://doi.org/10.1080/02724634.2017.1318284

Wang, W., Liao, W., Li, D., Tian, F., 2014. Early Pleistocene large-mammal fauna associated with Gigantopithecus at Mohui Cave, Bubing Basin, South China. Quaternary International, Multidisciplinary Perspectives on the Gigantopithecus Fauna and Quaternary Biostratigraphy in East Asia 354, 122–130. https://doi.org/10.1016/j.quaint.2014.06.036

Water Isotopes Database [WWW Document], 2023. URL https://wateriso.utah.edu/waterisotopes/pages/spatial_db/SPATIAL_DB.html (accessed 10.25.23).

Westerhold, T., Marwan, N., Drury, A.J., Liebrand, D., Agnini, C., Anagnostou, E., Barnet, J.S., Bohaty, S.M., De Vleeschouwer, D., Florindo, F., 2020. An astronomically dated record of Earth's climate and its predictability over the last 66 million years. Science 369, 1383–1387.

What Did Lupe Eat? - Mammoth Discovery [WWW Document], n.d. URL https://www.cdm.org/mammothdiscovery/lupeeat.html (accessed 1.10.24).

Wheelock, N., 1980. Environmental Sodium as a Factor in the Behavior and Distribution of African Elephants. Elephant 1. https://doi.org/10.22237/elephant/1521731760

Wood, R., Fleury, A.B.C., Fallon, S., Nguyen, T.M.H., Nguyen, A.T., 2021. DO WEAK OR STRONG ACIDS REMOVE CARBONATE CONTAMINATION FROM ANCIENT TOOTH ENAMEL MORE EFFECTIVELY? THE EFFECT OF ACID PRETREATMENT ON RADIOCARBON AND δ13C ANALYSES. Radiocarbon 63, 935–952. https://doi.org/10.1017/RDC.2021.32

Wooller, M.J., Bataille, C., Druckenmiller, P., Erickson, G.M., Groves, P., Haubenstock, N., Howe, T., Irrgeher, J., Mann, D., Moon, K., Potter, B.A., Prohaska, T., Rasic, J., Reuther, J., Shapiro, B., Spaleta, K.J., Willis, A.D., 2021. Lifetime mobility of an Arctic woolly mammoth. Science 373, 806–808. https://doi.org/10.1126/science.abg1134

Wu, Y., Deng, T., Hu, Y., Ma, J., Zhou, X., Mao, L., Zhang, H., Ye, J., Wang, S.-Q., 2018. A grazing Gomphotherium in Middle Miocene Central Asia, 10 million years prior to the origin of the Elephantidae. Sci Rep 8, 7640. https://doi.org/10.1038/s41598-018-25909-4

Zachos, J., Pagani, M., Sloan, L., Thomas, E., Billups, K., 2001. Trends, rhythms, and aberrations in global climate 65 Ma to present. Science 292, 686–693.

Zachos, J.C., Dickens, G.R., Zeebe, R.E., 2008. An early Cenozoic perspective on greenhouse warming and carbon-cycle dynamics. Nature 451, 279.

Graphical abstract

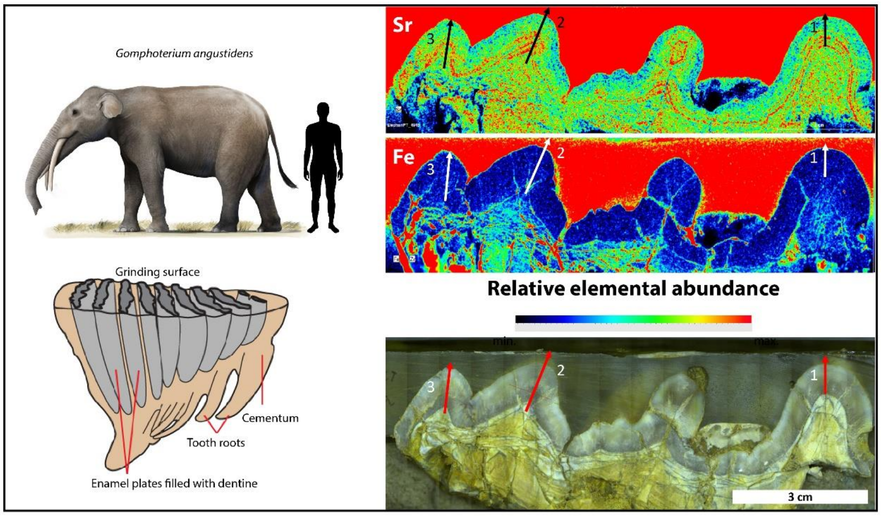

https://doi.org/10.5194/egusphere-2025-1770
Preprint. Discussion started: 11 June 2025

Figure 1_Coimbra et al.

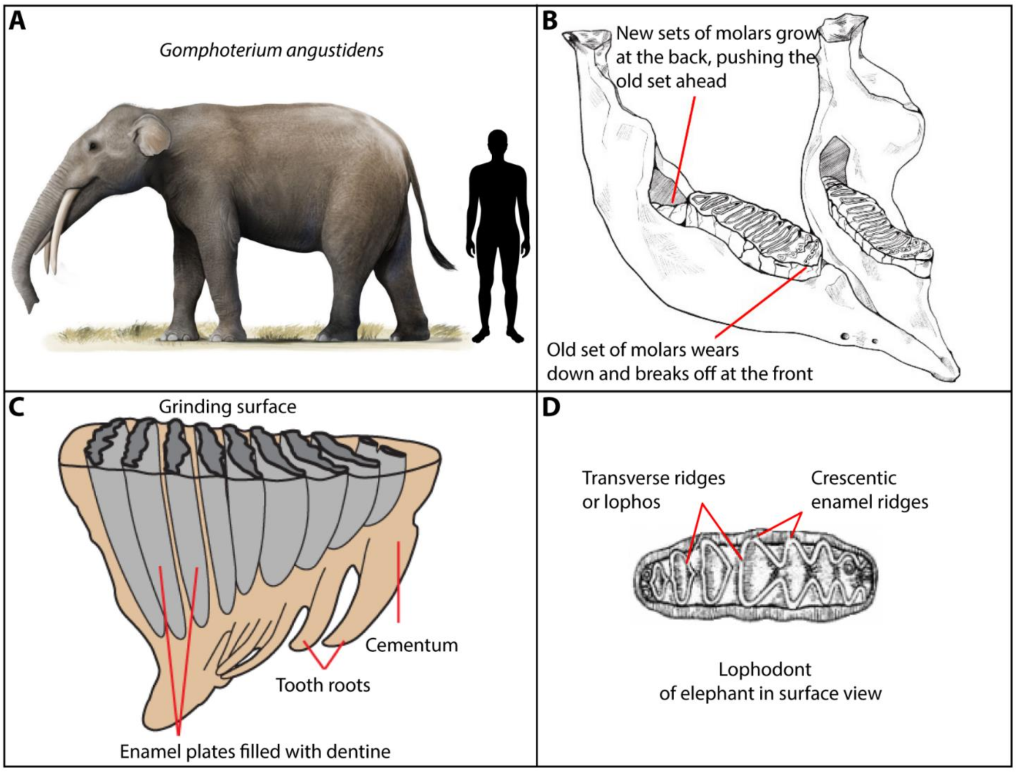

Figure 1. Relevant aspects of Proboscidean morphology and dental anatomy. A) Artistic illustration of *Gomphotherium angustidens* and scale relative to human silhouette (adapted from ("*Gomphotherium angustidens* by cisiopurple on DeviantArt," 2022), ©cisiopurple). B) Schematic representation of molar growth process (adapted from (Jayachandran, 2022) ©Wildlife SOS). C) Molar structure and relative distribution of enamel, dentine and cement (adapted from ("What Did Lupe Eat? - Mammoth Discovery," n.d.) ©Children's Discovery Museum, San Jose, USA). E) Lophodont of elephant in surface view, describing the intricate folding of enamel and dentine to form transverse ridges or lophs (adapted from Bhavya, 2017).

Figure 2_Coimbra et al.

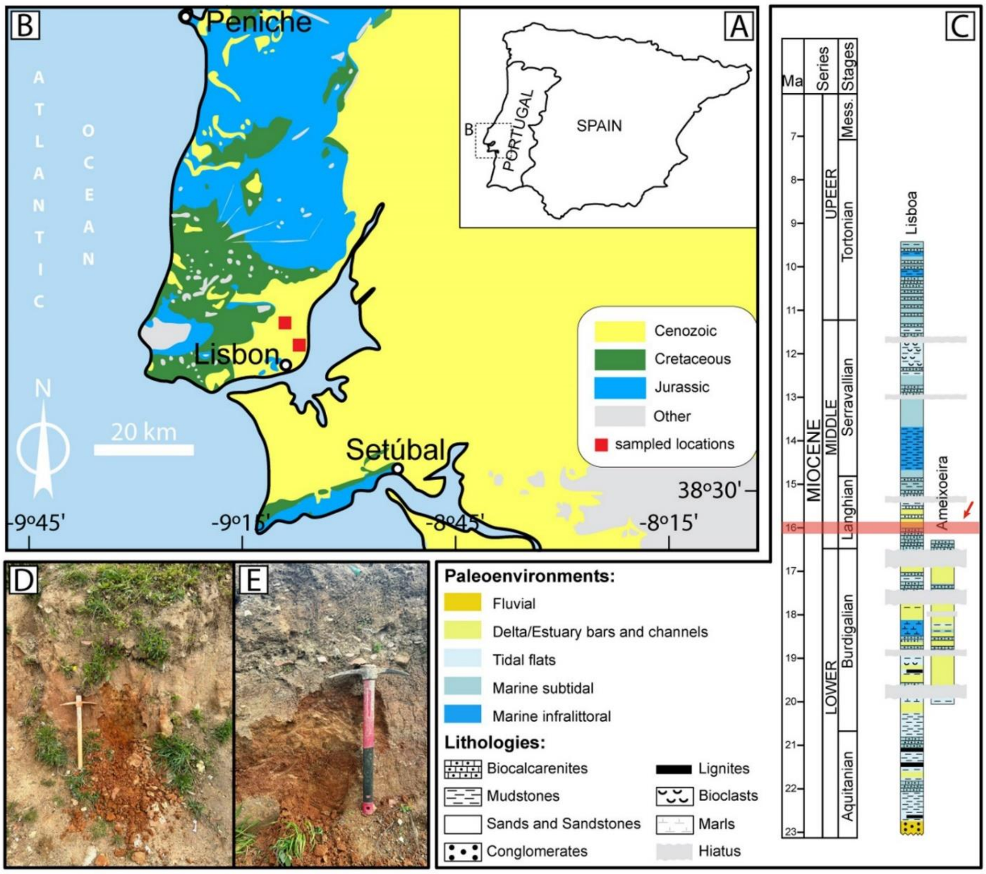

Figure 2. Geographical setting of the studied areas. A) Location of the Portuguese mainland in the Iberia Peninsula. B) Regional distribution of main geological outcrops at the Lisbon area (adapted from LNEG-LGM, 2010). Squares indicate the location of studied sections. C) General biochronostratigraphic scheme for the Miocene and stratigraphic context of studied deposits at the Lisbon area (adapted from Pais et al., 2012). D and E) Field aspect at the localities where the samples were extracted. The molars analysed in this study originate from the Quinta da Farinheira in the Lower Tagus Basin (Areias do Vale de Chelas, Lisbon). The Chelas unit has been designated SDL1 by Antunes & Ginsburg (2003) and Vb by Cotter (1956), with an estimated age of (~15.9–16.1 Ma) and is highlighted by a red arrow. It belongs to the Langhian stage and the MN5 biozone (13.7–16.0 Ma).

Figure 3_Coimbra et al.

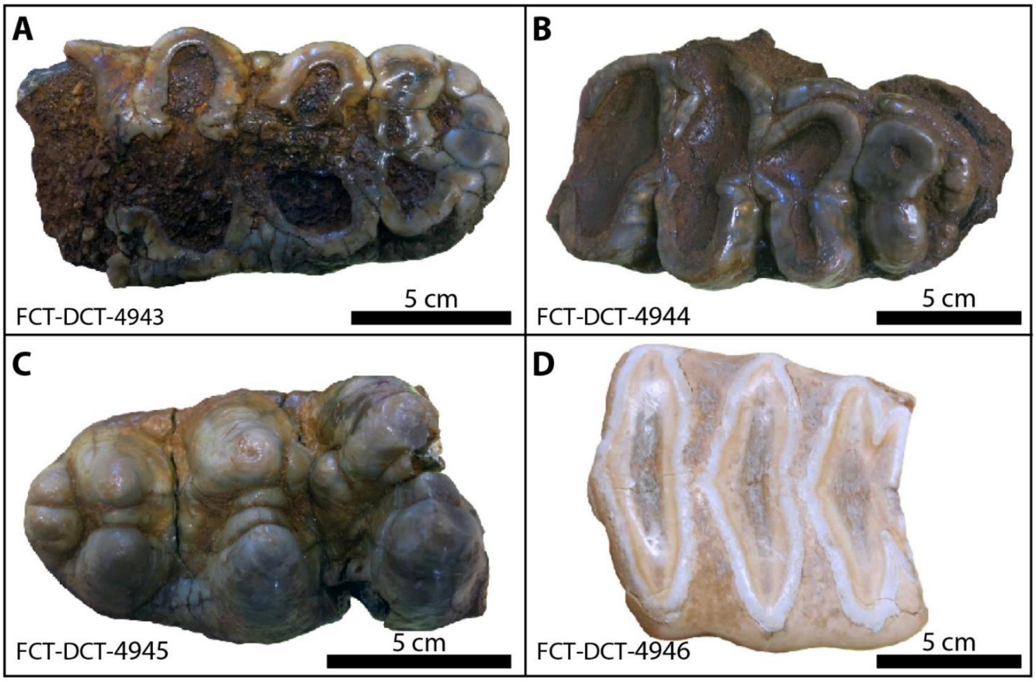

Figure 3. General aspect of uncut molar samples. A to C) *Gomphotherium angustidens* molars, note less significant wear of the collected samples from A to C. D) Modern L. Africana molar, showing typical diamond-shaped ridges.

Figure 4_Coimbra et al.

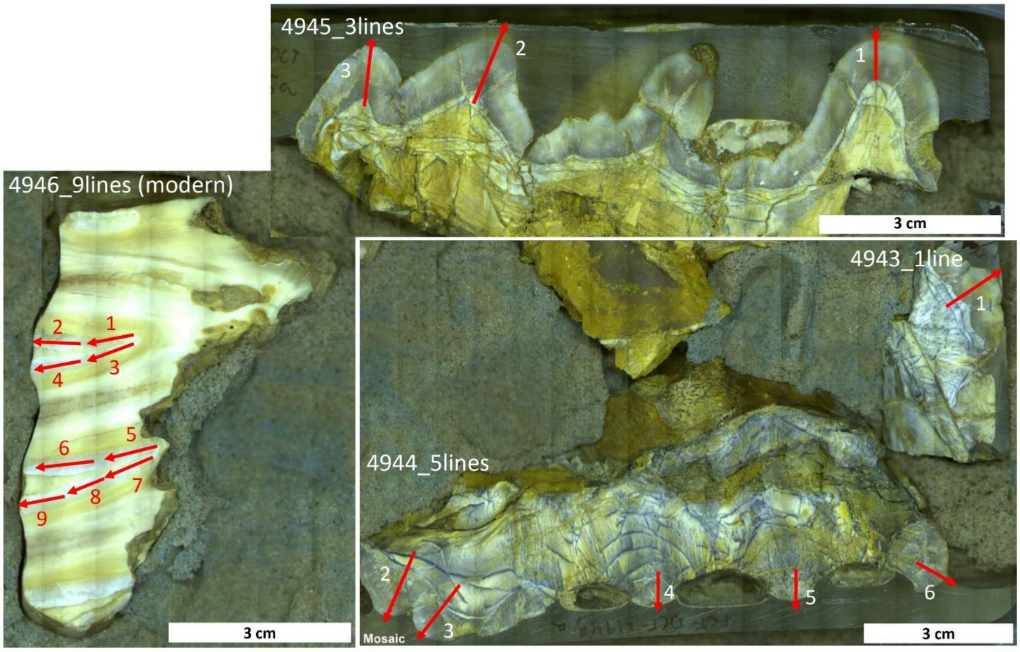

Figure 4. Microscope composite of longitudinally cut modern and Mid-Miocene molar samples with indication of elemental transects chosen for each section (red arrows). Note the inwards-outwards direction of all transects, along growth direction Specimen FCT-DCT 4945 in the top right, FCT-DCT 4933 bottom center and FCT-DCT 4943 on the far right. The modern elephant molar is depicted in the bottom left.

Figure 5_Coimbra et al.

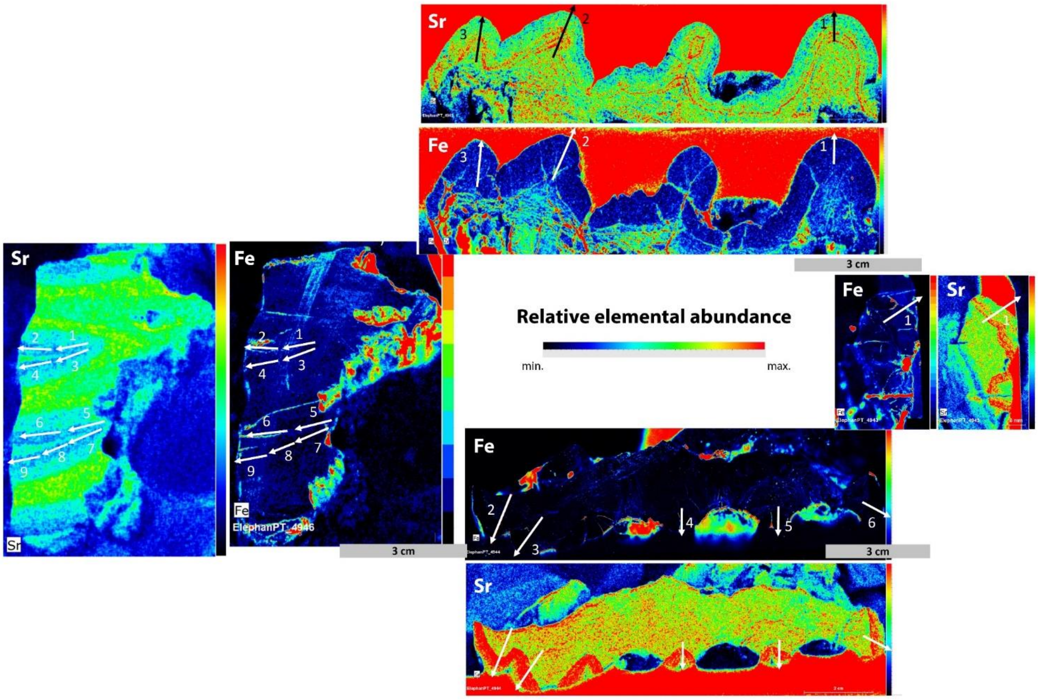

Figure 5. Relative elemental abundance for all specimen, here shown for iron and strontium (distribution of other elements can be found at https://doi.org/10.5281/zenodo.14882824). Note the lack of areas denoting higher iron abundance along selected transects and the clear Sr concentration pattern highlighting well-preserved tooth morphology.

Figure 6_Coimbra et al.

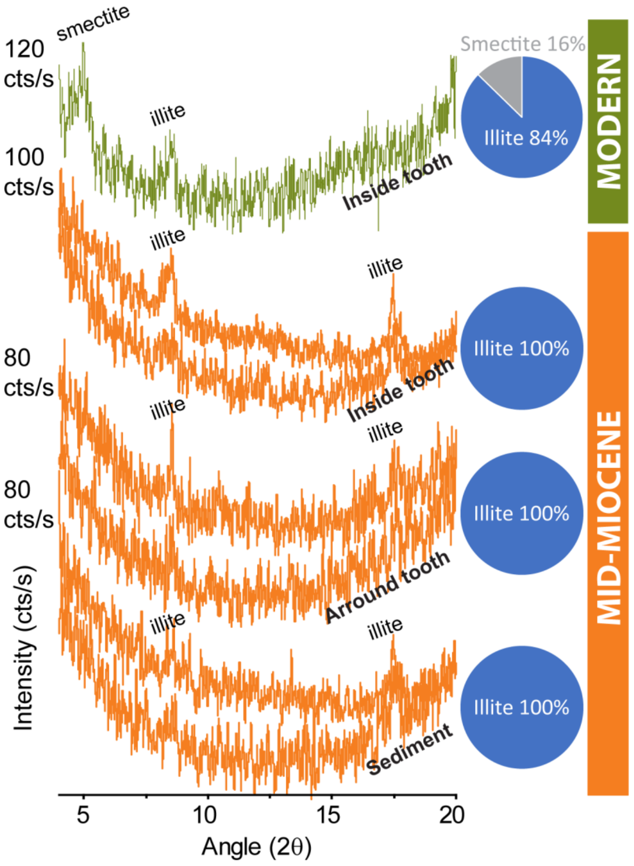

Figure 6. Clay mineral assemblage for Mid-Miocene sediment samples collected from areas adjacent to the molars, around and inside cavities. Modern sediment sample reflects soil substrate from the Lisbon Zoo (see text for details). Note the dominance of illite in all cases, along with minor contribution of smectite for the modern sample.

https://doi.org/10.5194/egusphere-2025-1770
Preprint. Discussion started: 11 June 2025

Figure 7_Coimbra et al.

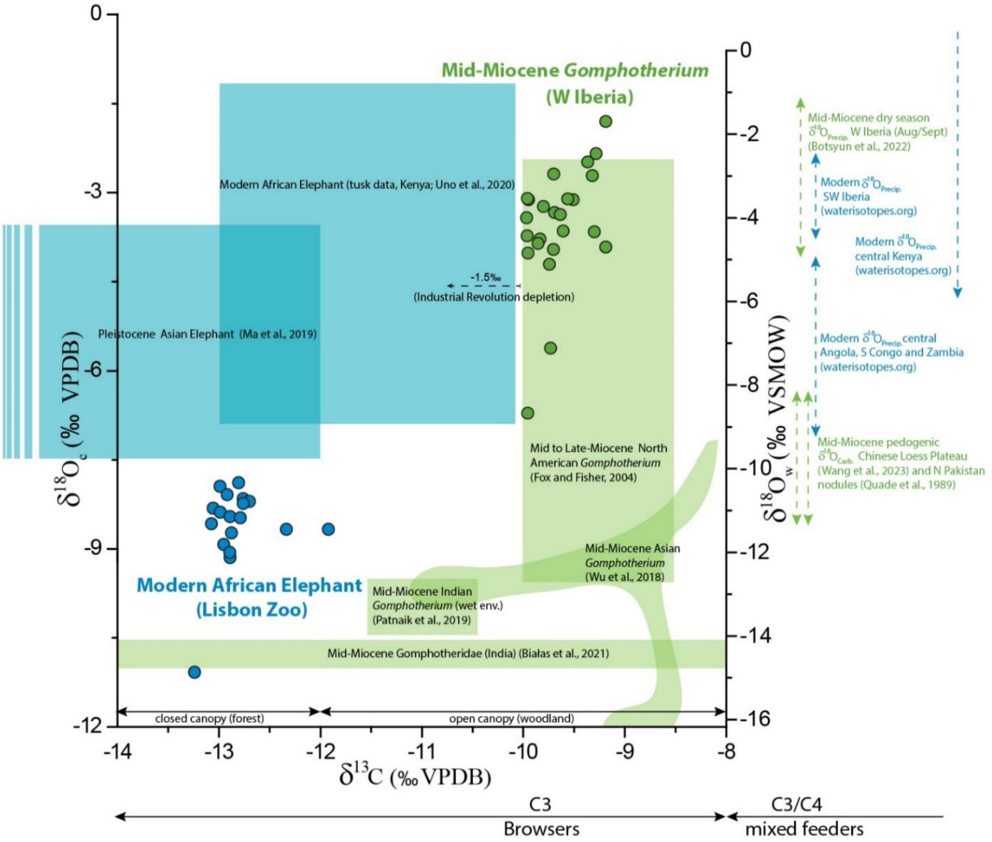

Figure 7. Biplot representation of stable carbon and oxygen isotope values, highlighting the differences between the two sets of samples tested (modern *vs.* Mid-Miocene). Shaded fields represent C and O isotope values in enamel-bound carbonate reported by other authors (see reference list) for Mid-Miocene and modern settings. Vertical arrows indicate range of variation of oxygen isotope values representative of rainfall composition at different localities (modern and ancient). Oxygen isotope values of water (right vertical scale) are compared to oxygen isotope values in bioapatite using the formula for large, water-dependent herbivores from (Hoppe, 2006) and we aligned the VSMOW to VPDB scale using the formula in (Coplen et al., 1983) following the methodology in (de Rooij et al., 2022) and (Wooller et al., 2021) . Forest/woodlands range of carbon-isotope variation after Patnaik et al. (2019) and references therein.

Figure 8_Coimbra et al.

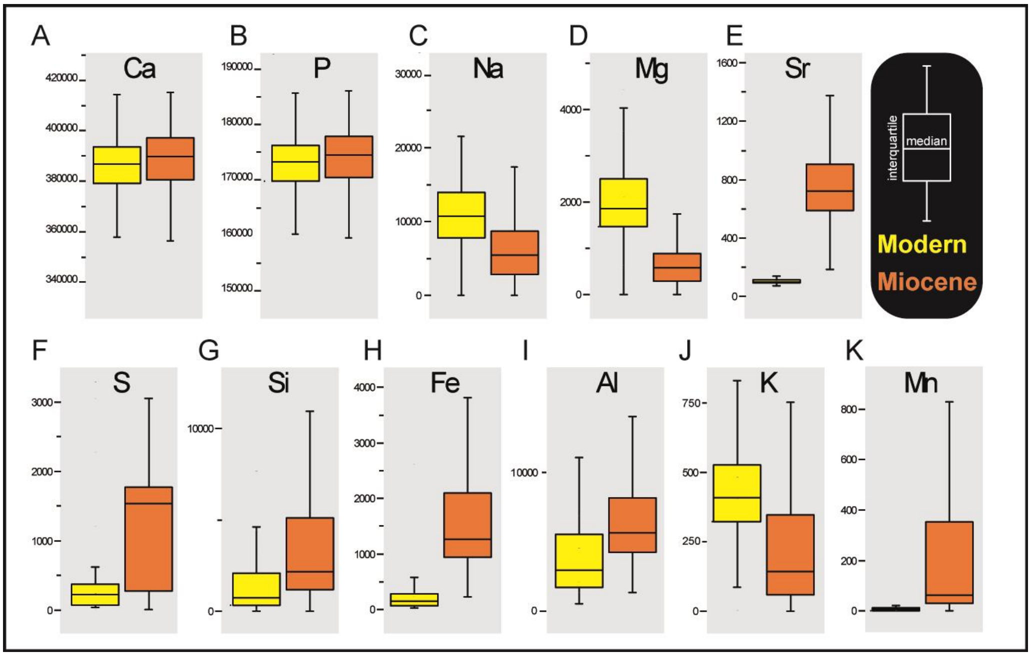

Figure 8. Boxplot representation (median and interquartile distance) of absolute elemental concentrations (in ppm). A and B) note similar distribution of Ca and P; C and D) lowered values for ancient samples regarding Na and Mg; E to K) overall higher median values for the remaining proxies (except K). See Table 2 for full elemental range, mean and standard deviation.

Figure 9_Coimbra et al.

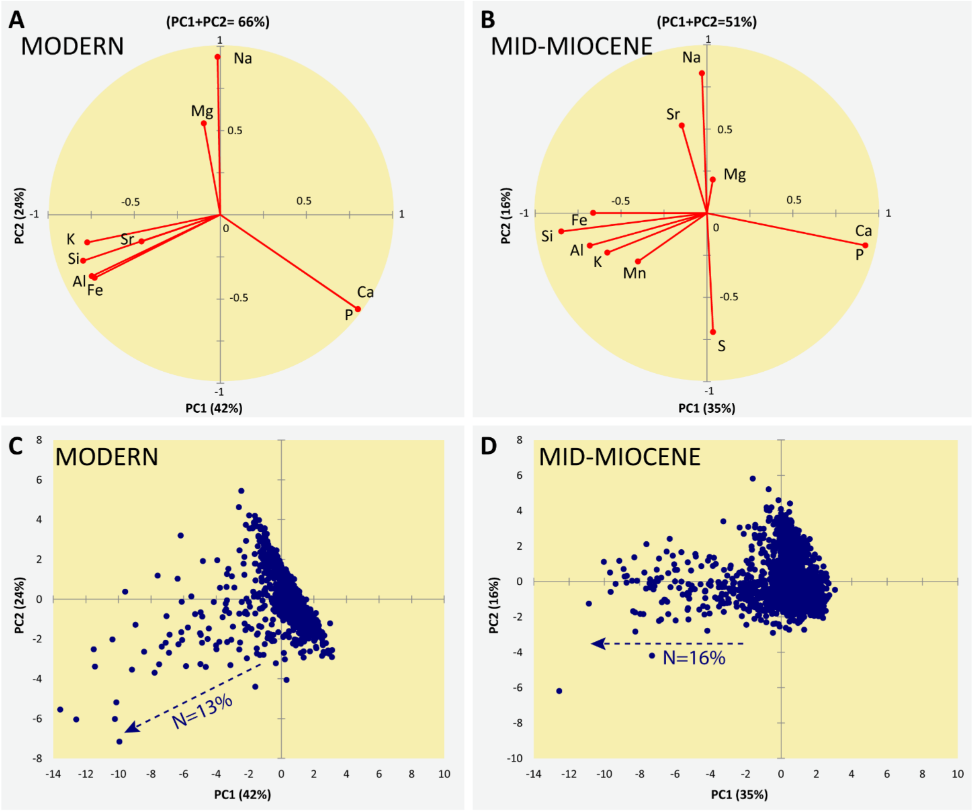

Figure 9. Principal component analysis computed for the modern and Mid-Miocene samples. A and B) Principal component loadings explaining 51 to 66% of the total variability of each set of samples. Note similar distribution of elements along the PC axis. Modern Mn and S were not used due to low number of measurements available (N<30%). C and D) Principal component scores indicating sample distribution along the PCA space. Note main clusters of samples in both cases, with only few samples (13% to 16% of the total number of samples) departing from the observed main trend.

Figure 10_Coimbra et al.

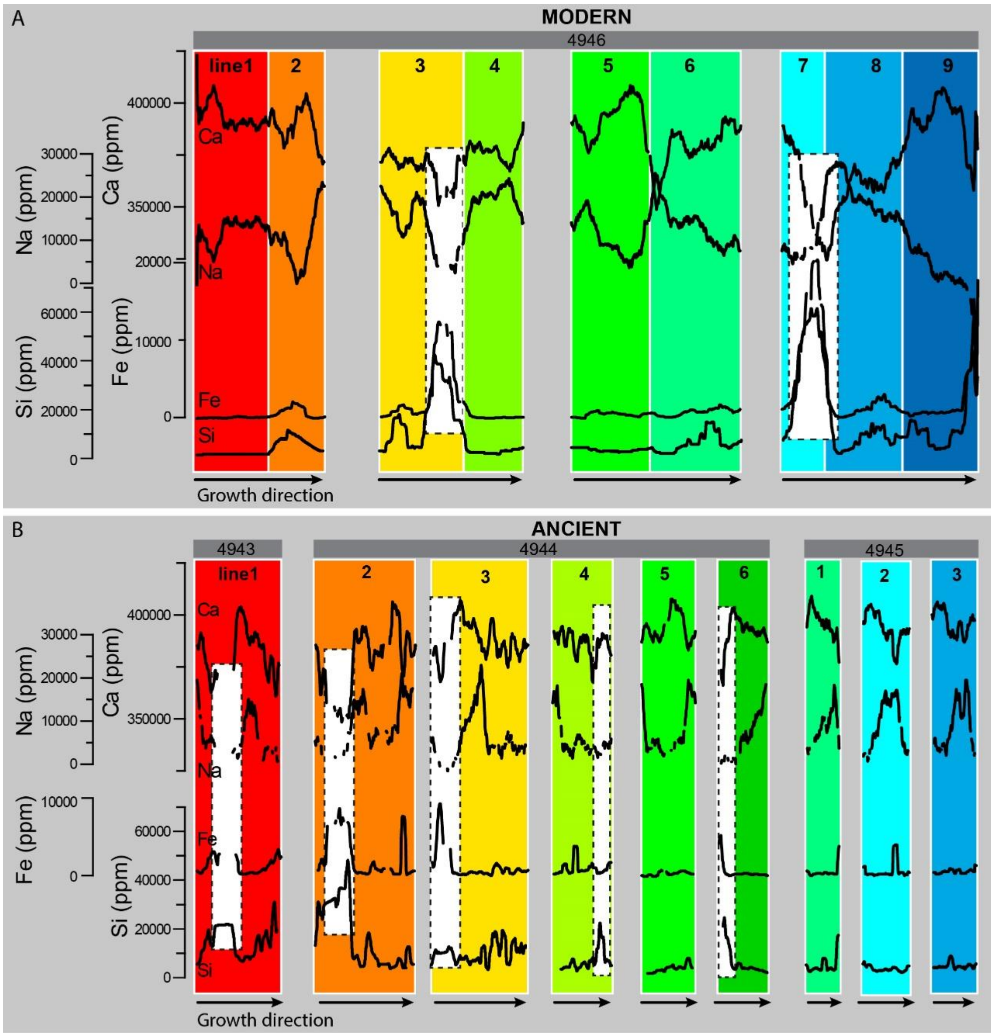

Figure 10. Elemental trend of selected proxies (Ca, Na, Fe and Si) for all measured transects (see Figs. 4 and 5 for exact measurement sites). A) Trend lines for modern transects. B) Trend lines for Mid-Miocene transects. Note overall similar records of Ca vs. Na and Fe vs. Si, as well as lack of clear enrichment or depletion trends along each transect. Note opposite variation pattern for Ca and Na, except when Fe and Si become significantly higher (white dashed boxes). Trend lines smoothed (10 points adjacent averaging); numerals according to Figure 4. Colors represent the different enamel transects analyzed. The same color scheme is used consistently across all figures to maintain clarity and allow for easy comparison of the different lines or transects.

https://doi.org/10.5194/egusphere-2025-1770
Preprint. Discussion started: 11 June 2025

Figure 11_Coimbra et al.

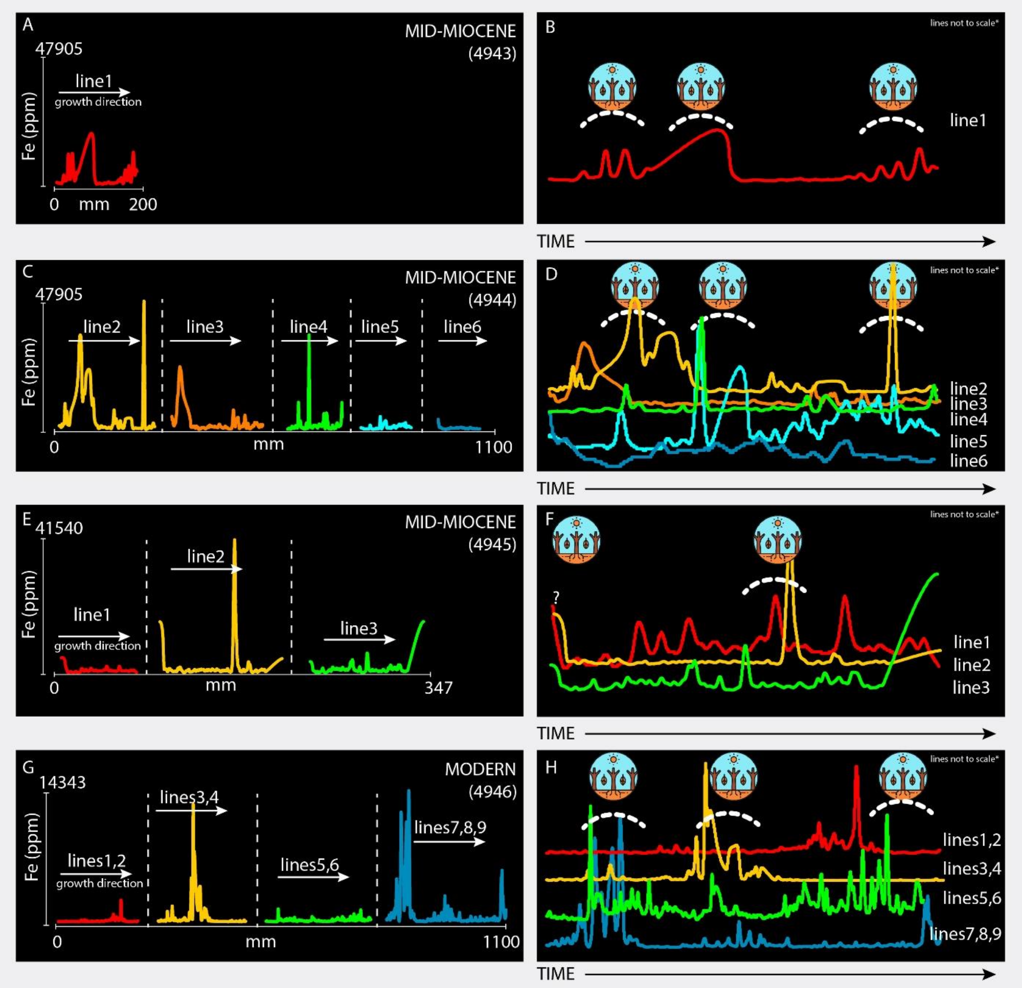

Figure 11. Elemental trend line obtained for Fe measurements (line numbers as in Figure 4). A, C E and G) Record of Fe abundance along growth direction (in mm). B, D F and H) Same datasets stacked and slightly adjusted (vertically and horizontally) to compare different transects that represent similar portions of the molar. (*) lines not to scale: mean horizontal scaling factor of 5.1; mean vertical scaling factor of 3.3 (see Table S1 in Appendix). Drawing represents dry season periods. Colors represent the different enamel transects analyzed. The same color scheme is used consistently across all figures to maintain clarity and allow for easy comparison of the different lines or transects.

https://doi.org/10.5194/egusphere-2025-1770
Preprint. Discussion started: 11 June 2025

Figure 12_Coimbra et al.

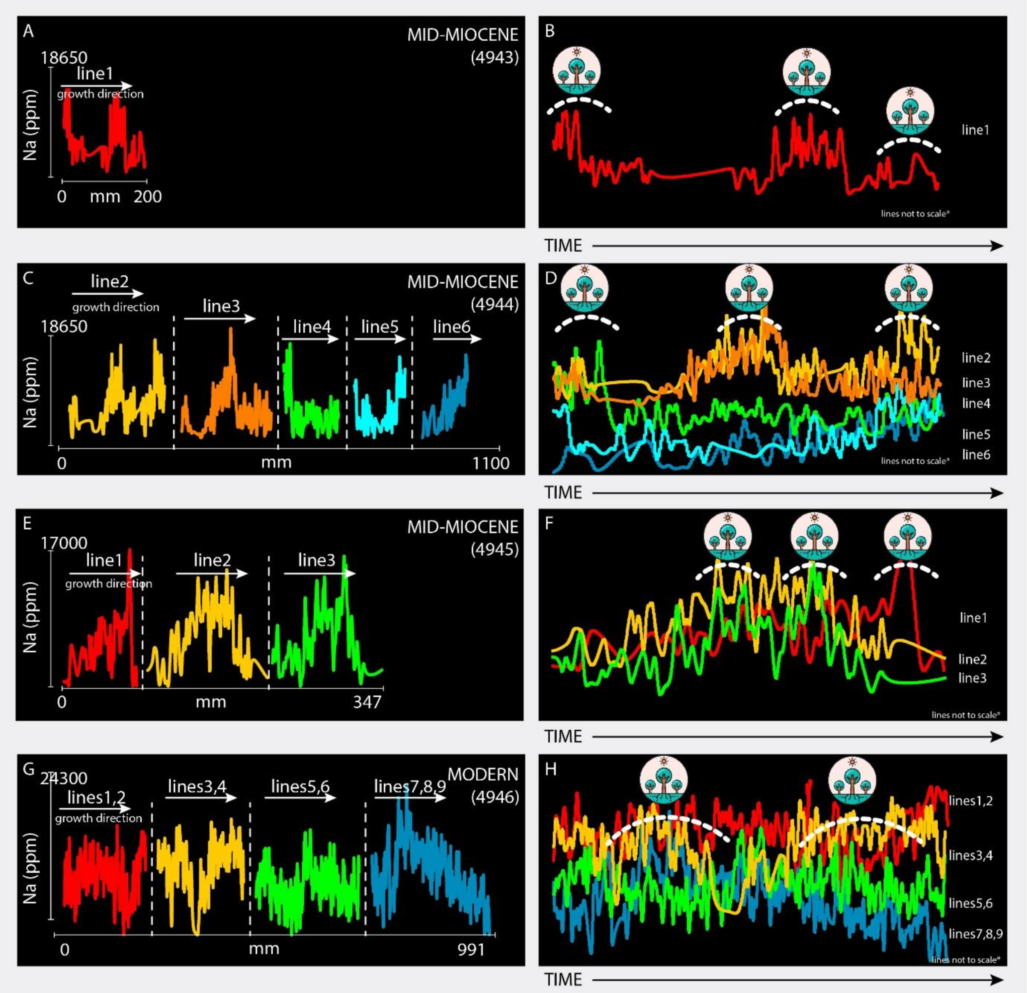

Figure 12. Elemental trend line obtained for Na measurements (line numbers as in Figure 3). A, C and E) Record of Na abundance along growth direction (in mm). B, D and F) Same datasets stacked and slightly adjusted (vertically and horizontally) to compare different transects that represent similar portions of the molar. (*) lines not to scale: mean horizontal scaling factor of 5.1; mean vertical scaling factor of 1 (see Table S1 in Appendix). Drawing symbol represents wet season periods. Colors represent the different enamel transects analyzed. The same color scheme is used consistently across all figures to maintain clarity and allow for easy comparison of the different lines or transects.

Figure 13_Coimbra et al.

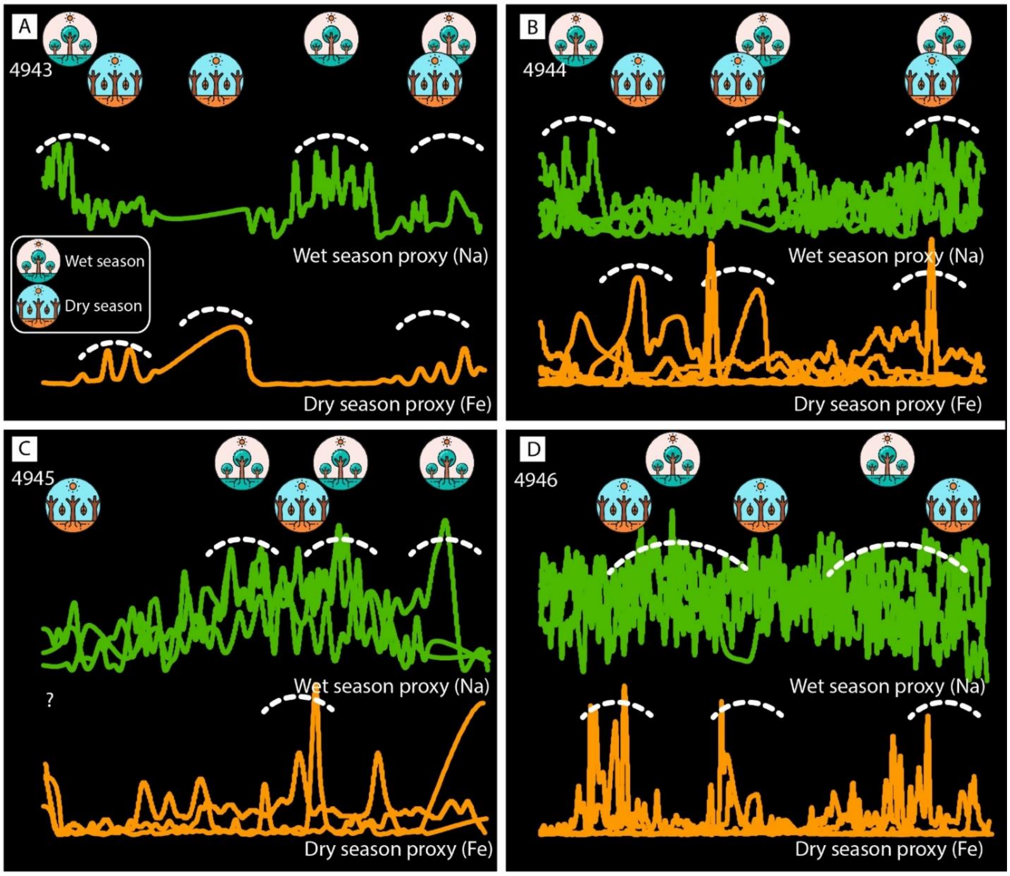

Figure 13. Compilation of elemental trend lines for Fe and Na as shown in Figures 11 and 12. A to C) Mid-Miocene transects in growth direction showing alternating peaks of higher abundance of the chosen elements. D) Modern transects in growth direction showing alternating peaks of higher abundance of the chosen elements.

Table 1. Semiquantitative abundance (%) of bulk mineralogical composition of sediment samples.

	Quartz	Calcite	Goethite	Ilmenite	Siderite	Dolomite	Observations
Sediment	96	1	3				yellow sediment
	94	2	4				hard crust
Arround Tooth	21		59	20			yellow sediment
	32		41			27	crust
Inside Tooth			100				red hard crust
	67		26		7		yellow sediment
Zoo	52	48					

Table 2. Mean (±standard deviation; s.d.), minimum and maximum elemental values obtained for selected proxies obtained from Miocene and modern samples.

Proxy	**Mean**	**s.d.**	**min.**	**Max.**	**Proxy**	**Mean**	**s.d.**	**min.**	**Max.**	**Proxy**	**Mean**	**s.d.**	**min.**	**Max.**
Ca	387428	14136	331284	415258	**Na**	6042	3982	8	22222	**Si**	4450	5944	3	44398
	385614	12089	331324	415589		10850	4459	2	26115		3278	7492	2	59156
P	173518	6331	148372	185982	**Mg**	645	465	1	4435	**Fe**	2621	4657	225	56135
	172706	5414	148391	186130		2383	1831	2	15502		428	1357	26	18381
					Sr	755	224	185	1510	**Al**	6891	4017	1332	25596
						107	34	63	722		4547	4825	512	45641
					S	1215	755	1	3046	**K**	403	701	0	5636
						246	164	40	617		485	342	85	4276
										Mn	506	1391	0	26942
											18	48	0	365

MIOCENE
MODERN